SF 298 MASTER COPY KEEP THIS COPY FOR REPRODUCTION PURPOSES

# REPORT DOCUMENTATION PAGE

*Form Approved*
*OMB NO. 0704-0188*



| 1. AGENCY USE ONLY *(Leave blank)* | 2. REPORT DATE | 3. REPORT TYPE AND DATES COVERED |
|---|---|---|
| | October 1997 | Final Progress Report, 9/94 - 2/97 |

**4. TITLE AND SUBTITLE**

Electronic Imaging

**5. FUNDING NUMBERS**

DAAH04-94-G-0323

**6. AUTHOR(S)**

Dr. Nicholas George, Principal Investigator
Wilson Professor of Electronic Imaging

**7. PERFORMING ORGANIZATION NAMES(S) AND ADDRESS(ES)**

**The Institute of Optics**
**University of Rochester**
**Rochester, NY 14627**

**8. PERFORMING ORGANIZATION REPORT NUMBER**

**9. SPONSORING / MONITORING AGENCY NAME(S) AND ADDRESS(ES)**

U.S. Army Research Office
P.O. Box 12211
Research Triangle Park, NC 27709-2211

**10. SPONSORING / MONITORING AGENCY REPORT NUMBER**

ARO 30402.1-PH

**11. SUPPLEMENTARY NOTES**

The views, opinions and/or findings contained in this report are those of the author(s) and should not be construed as an official Department of the Army position, policy or decision, unless so designated by other documentation.

**12a. DISTRIBUTION / AVAILABILITY STATEMENT**

Approved for public release; distribution unlimited.

**12 b. DISTRIBUTION CODE**

**13. ABSTRACT** *(Maximum 200 words)*

Theoretical and experimental research was proposed on topics of strategic importance in electronic imaging with an emphasis on problems of basic research significance which also have relevance to novel systems for imaging, automatic pattern recognition, and remote sensing. Our goal has been to make contributions in imaging science that will lead to a better understanding of hybrid systems combining optical imaging, photosensors, and digital computers for signal processing. In the statement of work we had proposed research on three related topics. First, we proposed to study the controlled blurring caused by an idealized point spread function, i.e., the random-walk or speckle-like psf. This novel method for controlled blurring appears to be useful in secure transmission and in image compression; and this psf has many interesting mathematical properties that we have investigated. Secondly, we proposed a study of image recovery in the Fresnel-zone (incoherent case) when the imaging system is misfocused. We applied modern coherence theory together with current computer-science techniques in order to obtain optimal recovery and, as well, to establish theoretical limits on the image quality of the restoration. In this research we also established an operator-independent method for the identification of the focusing errors. For the third topic, we had intended to continue with the remote sensing of particulates to include extension of the inversion theory (formulated in 1990-1991) to the case of moving aerosols. Unfortunately, work in this area has not progressed as we had hoped, yet future plans remain to include the use of variable wavelength as a tool in particulate diagnostics.

**14. SUBJECT TERMS**

Random-walk, point spread function, image processing, speckle, defocus blur, Fresnel zone, lensless imaging, image quality, particulate sizing, particulate distribution

**15. NUMBER IF PAGES**

**16. PRICE CODE**

| 17. SECURITY CLASSIFICATION OR REPORT | 18. SECURITY CLASSIFICATION OF THIS PAGE | 19. SECURITY CLASSIFICATION OF ABSTRACT | 20. LIMITATION OF ABSTRACT |
|---|---|---|---|
| UNCLASSIFIED | UNCLASSIFIED | UNCLASSIFIED | UL |

NSN 7540-01-280-5500

Standard Form 298 (Rev. 2-89)
Prescribed by ANSI Std. 239-18
298-102

# Electronic Imaging

## Table of Contents

# Electronic Imaging

## Abstract

Theoretical and experimental research was proposed on topics of strategic importance in electronic imaging with an emphasis on problems of basic research significance which also have relevance to novel systems for imaging, automatic pattern recognition, and remote sensing. Our goal has been to make contributions in imaging science that will lead to a better understanding of hybrid systems combining optical imaging, photosensors, and digital computers for signal processing. In the statement of work we had proposed research on three related topics. First, we proposed to study the controlled blurring caused by an idealized point spread function, i.e., the random-walk or speckle-like psf. This novel method for controlled blurring appears to be useful in secure transmission and in image compression; and this psf has many interesting mathematical properties that we have investigated. Secondly, we proposed a study of image recovery in the Fresnel-zone (incoherent case) when the imaging system is misfocused. We applied modern coherence theory together with current computer-science techniques in order to obtain optimal recovery and, as well, to establish theoretical limits on the image quality of the restoration. In this research we also established an operator-independent method for the identification of the focusing errors. For the third topic, we had intended to continue with the remote sensing of particulates to include extension of the inversion theory (formulated in 1990-1991) to the case of moving aerosols. Unfortunately, work in this area has not progressed as we had hoped, yet future plans remain to include the use of variable wavelength as a tool in particulate diagnostics. This program of research has been heavily leveraged by cost participation from the University of Rochester, the industrial sponsors of the Center for Electronic Imaging Systems, the New York State Science and Technology Foundation, and the National Science Foundation.

# Electronic Imaging

# Section 2: Technical Progress Report

In the following sections we present descriptions of three related research topics, starting each with a statement of the problem and then a summary of important results.

## 2.1 The Random-walk point spread function

### 2.1.1 Statement of the Problem

In electronic imaging topics of major interest are the transmission and storage of high resolution images. Then, in cases where atmospheric turbulence leads to blurring, we would like to discover image recovery methods that are effective in restoring high quality images. Additionally, it may be possible to blur images in a simple controlled way in order to provide security or better image compression which would be useful both in transmission and storage. As a topic of basic research, we believe that a study of controlled blurring caused by a novel point spread function consisting of 25 to 250 randomly distributed delta functions will lead to important theoretical results in speckle, in function theory, and in image recovery. Moreover, this study will lead ultimately to better methods for recovering images degraded by atmospheric turbulence. One research objective is to study image recovery methods using the controlled blurring caused by a random-walk point spread function. We would also like to study other blur functions particularly in regard to the occurrence of zeros in their spatial Fourier transform. Hopefully, we will discover several important new point spread functions that are useful for controlled blurring. Related objectives are to seek to establish a useful quantitative measure of image quality and to contribute to an understanding of better methods for image compression.

### 2.1.2 Summary of Results

In the time frame of this report Bryan Stossel completed his thesis titled "Image Processing, Coding, and Compression with Multiple-Point Impulse Response Functions" and received his Ph.D. in 1994. The multiple-point impulse response is unique among degradations in imaging systems. Most other degradations have transfer functions that can become very small or go to zero at many spatial frequencies. This results in errors in the recovery when the degraded image is divided by this transfer function. The randomness of the multiple-point impulse response gives a zero in the transfer function once in only 1000 realizations. Thus the reconstructions are virtually error-free. An added benefit is that this makes the multiple-point impulse response an ideal tool for image coding and compression since the blurred image

contains much less high frequency detail than the original image and therefore can be compressed to much higher ratios than the original without loss of information. And unless the exact point spread function is known, reconstructing the original image is virtually impossible resulting in highly secure data encryption. A patent and several publications have resulted from this work.

## 2.2 Image Recovery and Blur Identification in the Fresnel Zone

### 2.2.1 Statement of the Problem

Image restoration deals with the estimation of the sharp image from a recorded image which is degraded by blurring and noise. Most restoration methods assume that the blur is known a priori. In some practical situations, the type of blur may be known, e.g., out-of-focus, but the amount of blurring may be unknown and may need to be estimated before restoring. We propose to investigate the blur identification problem in four stages.

**Stage 1:** As a topic of central importance in imaging science, one needs to establish theoretical bounds to image restoration from blurred samples taken at various planes in the Fresnel zone. Our approach to this is to apply modern coherence theory to the computer science methodologies in order to devise optimal recovery methods and to establish theoretical limits. An image quality metric will be employed in order to measure the recovered images. In this phase of the research, we are fortunate to have the participation by Professor Emil Wolf.

**Stage 2:** We propose a neural network approach to the identification of the amount of defocus in recorded images. This approach is motivated by the successful application of neural networks to solving pattern recognition problems.

**Stage 3:** Another goal is to perform a comparative study of blur identification methods. Despite the attention that the blur identification problem has recently received, there is no single comparative study of the existing blur identification methods. The objective of the proposed study is to compare the existing blur identification methods by evaluating (i) their applicability to various blur types, (ii) their performance in the presence of noise, and (iii) their computational efficiency.

**Stage 4:** We will finally investigate the identification of blurs due to depth of field. We propose to apply sectioned methods based on the local Fourier transform. We also propose to investigate the wavelet transform as an alternative to the local Fourier transform. The objective of this study is to segment the degraded image based on the amount of defocus on each section, and utilize this information in image restoration.

### 2.2.2 Summary of Results

A theoretical analysis has been performed for image retrieval when a planar transparency is illuminated by spatially incoherent light that propagates in free space and is then recorded on a CCD array, but without using an imaging lens. Based on Maxwell's equations and Fourier-optical, linear-systems theory, equations were derived for digital processing of this badly blurred image in order to recover a reasonable facsimile of the original. Rigorous impulse responses and their corresponding transfer functions were derived for the cases of general amplitude illumination and for incoherent illumination. With exact results in the framework of Maxwell's equations, we found that free-space propagation from a planar aperture is space-invariant in general. One main theme was to derive a rigorous expression for the optical-transfer-function of free space, and thereby secondly to study the feasibility of image retrieval using a lensless recording system and post digital processing. We found the interesting result that this intensity based transfer function consists principally of a modified Bessel function of the second kind, $K_1(v)$, which is well known not to have any zeros for finite real values of its argument. The significance of this is that recovery of the pictorial image is likely using digital processing means. A paper on this subject has been published.

We have successfully sorted a scene-independent set of images based on blur level using a computer for automatic assessment of image quality. The research was then extended to use a neural network. The network was trained to sort the images according to blur level and a high correlation was achieved with a human visual assessment. A paper was presented at the 47th Annual IS&T Conference in 1994.

## 2.3 Retrieval of Spatial Distribution and Size of Particles

### 2.3.1 Statement of the Problem

Particle measurements are of special importance in the study of combustion processes, pollution control, biological experiments and many other military and industrial applications. Optical techniques based on diffraction with laser illumination are most frequently used among all optical and non-optical methods. The optical measurement requires an inversion process to reconstruct information of particle samples, such as size, shape and spatial distribution. Different methods, including direct integral transforms, matrix inversions and iteration algorithms, have been studied in past decades and most of them are used solely for particle sizing. As early as in 1955 Shifrin developed the original integral-transform method for recovering the size-distribution function from the optical transform intensity of a spherical particle. However, little success was obtained in early applications of this inversion method mainly due to the existence of speckles in the scattered field. The invention

of the ring-wedge photodetector in 1970 resolved the speckle problem and has been since applied widely to optical particle-size measurements. Matrix-inversion techniques have been used to analyze the intensity information obtained by ring detectors. The main weakness of matrix inversion is its susceptibility to noise, so it does not provide reliable particle-size distributions especially when the number density of particles is low. Our recent study presents an improved theory for the inversion formula and interesting new experiments of the resolution in size **vs**. the sampling angle. Compared with Shifrin's first formula the current formula does not contain a derivative of the measured intensity and is less susceptible to noise. Experiments using the ring-wedge detector and this inversion formula to recover different particle-size distributions show excellent agreement with the theory.

We propose to extend our study of the remote sensing of particulates, as follows. Besides size distribution, the remote sensing will include recovering information about spatial location, speed, and number-density distributions of the scattering particles.

### 2.3.2 Summary of Results

For the third topic, we had intended to continue with the remote sensing of particulates to include extension of the inversion theory (formulated in 1990-1991) to the case of moving aerosols. Unfortunately, work in this area has not progressed as we had hoped, yet future plans remain to include the use of variable wavelength as a tool in particulate diagnostics.

# SECTION 3: PATENTS AND PUBLICATIONS

## Patents

"Image data coding and compression system utilizing controlled blurring," Nicholas George and Bryan J. Stossel, U.S. Patent No. 5,453,844, September 1995.

## Publications*

"The blurred bird," Nicholas George and Bryan J. Stossel, Technical Note, 1993.

"Automatic image quality assessment," David M. Berfanger and Nicholas George, IS&T's 47th Annual Conference/ICPS 1994, 436-438 (1994).

"Controlled blurring in image processing," Bryan J. Stossel and Nicholas George, IS&T's 47th Annual Conference/ICPS 1994, 534-535 (1994).

"Object recognition and image coding," Nicholas George, B. J. Stossel, and D. M. Berfanger, invited paper presented at Takayanagi Memorial Session, Asia Display '95, Hamamatsu, Japan, October 1995.

"Multiple point impulse responses: controlled blurring and recovery," Bryan J. Stossel and Nicholas George, Opt. Comm. **121**, 156-165 (1995). *Erratum*, Opt. Comm. **122**, 212 (1996).

"Lenless electronic imaging," Nicholas George, Opt. Comm. **133**, 22-26 (1997).

"Effective transmission of speckled images using controlled blurring," Nicholas George and Jun Ren, IEEE Trans. on Ultrasound, xxx, pp (1997), in review.

*Copies of journal articles can be found in the Appendix.

## SECTION 4: PARTICIPATING SCIENTIFIC PERSONNEL

**Nicholas George**, Principal Investigator; Director, NSF-NYSSTF S/IUCRC Center for Electronic Imaging Systems; Director, ARO-URI Center for Opto-Electronic Systems Research; Wilson Professor of Electronic Imaging; Professor of Optics; and Professor of Electrical Engineering

**Shen-Ge Wang**, Scientist in Optics

Dr. Wang received his Ph.D. in 1986. Thesis title: "Optical transforms in white light."

(Dr. Wang is now a scientist at Xerox Corporation, Webster, NY)

**Donald J. Schertler**, Scientist in Optics, Center for Electronic Imaging Systems

Dr. Schertler received his Ph.D. in 1993. Thesis title: "Wavelength and roughness dependence of backscattering"

**Bryan J. Stossel**, Scientist in Optics

Dr. Stossel received his Ph.D. in 1994. Thesis title: "Image processing, coding, and compression with multiple-point impulse response functions."

(Dr. Stossel is now a scientist at Eastman Kodak Company, Research Laboratories, Rochester, NY)

**Stojan Radic**, Scientist in Optics

Dr. Radic received his Ph.D. in 1995. Thesis title: "Periodic structures in multiwavelength optical systems."

(Dr. Radic is now a scientist at Corning, Inc., Corning, NY)

**David M. Berfanger**, Ph.D. Fellow.

Anticipated date of Ph.D. is May 1998. Thesis title: "Automatic pattern recognition using an all digital ring-wedge detector."

**William Wade Cook**, Ph.D. Fellow.

Anticipated date of Ph.D. is August 2000. Thesis topic: holographic contouring of large objects

**Damon Diehl**, Ph.D. Fellow.

Anticipated date of Ph.D. is May 2001. Thesis topic: holographic optical switch

**Jun Ren**, M.S. Fellow.

Ms. Ren received her M.S. in April 1997. Master's title: "Atomic force microscopy"

**Gregory S. Kaufman**, Technical Computer Assistant

**Wendell Allen Neff**, Ph.D. Fellow

Anticipated date of Ph.D. is _____. Thesis topic:

# APPENDIX — PUBLICATIONS

UNIVERSITY OF
ROCHESTER

COLLEGE OF ENGINEERING AND APPLIED SCIENCE
THE INSTITUTE OF OPTICS

# THE BLURRED BIRD

Nicholas George and Bryan J. Stossel
Center for Electronic Imaging Systems
The University of Rochester

29 October 1993

In a long-term study of image recovery for atmospherically degraded images, Nicholas George and Bryan Stossel have been investigating an idealized multiple-point impulse response. For theoretical purposes they assert a multiple-point impulse response, similar to speckle stellar interferometry in which a single impulse is imaged as, say, 25 to 200 randomly spaced delta functions. Pictorially the effect is as shown in the accompanying photographs with the blurred object as shown. It appears visually as though shrouded in fog, certainly it is blurred far beyond recognition. In theoretical terms it is readily shown that the spatial frequencies in the blurred image have been reshaped with the high frequency content being greatly reduced by the ratio 1/N, where N is the number of points in the random-walk impulse response.

An almost perfect image recovery is possible using an inverse filter generated by taking the two-dimensional spatial Fourier transform (FFT) of the degrading impulse response. Division of the FFT of the blurred object's intensity leads to an almost perfect recovery. It is surprising that a simple inverse filter is so effective, since in many other image recovery situations, contours of zeros in the Fourier transform leads to indeterminancies in the calculation of the recovered image. For the random-walk blur, these researchers have shown that the FFT has only discrete zeros with a computational chance of

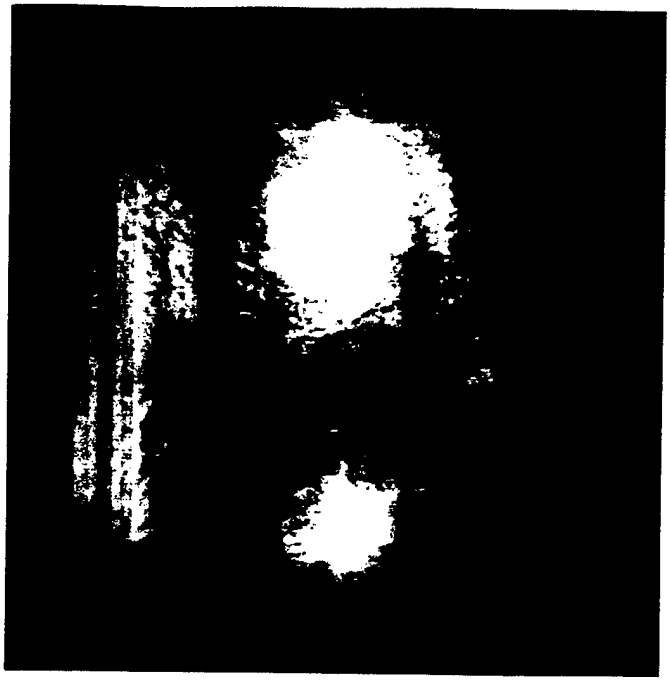

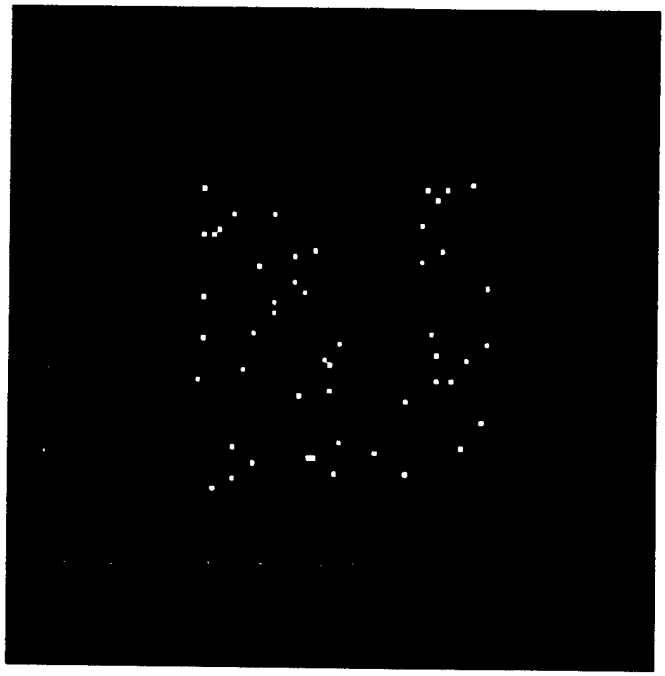

running into a zero thereby greatly reduced. They estimate some trouble with the image recovery once in ten thousand frames.

Two interesting commercial applications of this research are being pursued. Since the high frequency detail is no longer apparent in the blurred image, it is reasonable to conjecture that FAX transmission of the images would require less space-bandwidth product than before. Using commercially available discrete-cosine-transform routines, these researchers have found that it is much easier to transmit the blurred bird than the original. Estimates for improved transmission, reduced pixels, are from two to four times.

Secondly, transmission of the blurred object gives the sender a degree of privacy. With the widespread increase of FAX for color photographs, it is becoming increasinglt important to provide some degree of privacy in transmission, particularly for commercial art in advertising displays. Related experiments are presently being conducted for the coding and transmission of engineering drawings and topographic maps.

This research is being supported by the Directorate of Physics of the U. S. Army Research Office.

# Automatic Image Quality Assessment†

*David M. Berfanger and Nicholas George*
*The Institute of Optics*
*University of Rochester*
*Rochester, NY 14627*

## Introduction

Psychovisual methods of image quality assessment, such as those described by Roufs, have a high correlation between observers and are widely considered the standard by which all other measures of image quality are compared.[1] The development of automated methods of image quality assessment have reflected this. Grogan and Keene have developed a method of image quality measurement based on a computational model for the human perception of image brightness.[2] Nill and Bouzas have presented an image quality measure based on the digital image power spectrum, which includes a model for the modulation transfer function of the human visual system.[3] Saghri, Cheatham, and Habibi have presented a preliminary image quality measure which takes into account both the illumination level sensitivity and the spatial frequency sensitivity of the human visual system.[4] Davies, Rose, and Smith have described an automatic image quality meter incorporating a model of the human visual system derived from both psychophysical and neurophysiological studies.[5]

In our research a principal concern is to establish limits on automatic, operator-independent, image quality assessment with the goal of determining whether computerized systems can perform at the level of a human observer when assessing images widely varying in scene content. In this report we are considering the possibility of using diffraction pattern sampling in combination with neural network software in the assessment of image quality. Our approach will be to present two preliminary, illustrative experiments. The first experiment uses a simple data base obtained from professional stock photography and degraded using various levels of computer-generated blurring. We study this sorting task for academic purposes. The second experiment involves a limited data base obtained from the Eastman Kodak company that was created using various lossy-compression and retrieval techniques and was accompanied by visual quality ratings made by trained photointerpreters. Preliminary results for both experiments are promising.

---

† *Research supported in part by the National Science Foundation , the NYS Science and Technology Foundation and the Army Research Office.*

## Diffraction Pattern Sampling and Neural Network Software

Diffraction pattern sampling is an optical technique of spectral analysis based on the properties of the Fourier spectrum of a real image. Earlier experiments have been described in which diffraction pattern sampling has been used successfully to implement image quality metric algorithms [6-8], and diffraction pattern sampling in connection with neural network software has also been used successfully to classify finger prints, faces, and particulate suspensions, as well as to distinguish differences between dogs and cats. [9, 10] The optical portion of the diffraction pattern sampling system is shown in Fig. 1. Coherent illumination is provided by a laser beam that is expanded and collimated by a spatial filter and a collimating lens. A neutral density filter is used to control the intensity. The object plane is adjacent to an optical transform lens. A ring-wedge detector is centered in the back focal plane of the transform lens. [6] The output signals from this detector are amplified, digitized, and sent to a digital computer for further processing.

For the experiments in this paper, diffraction pattern sampling is digitally simulated using a standard FFT algorithm, and the resulting ring-wedge data is provided to neural network software for quality sorting tasks. This simulation is to be described more fully in a separate publication. The use of neural network software allows the study of differing network structures both before and after training; furthermore, in choosing appropriate data sets and in pre-selecting what information is given to the network, we believe it possible to obtain a better understanding of what measurable aspects of an image contribute to its perceived quality.

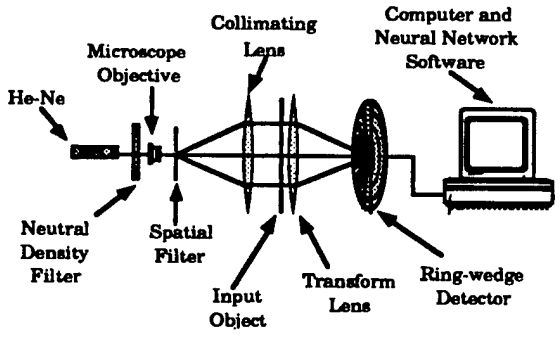


*Figure 1. Block diagram of the optical portion of the diffraction pattern sampling system.*

### Sorting Blur Level

As a first step in our research, a preliminary experiment was conducted for the specific task of sorting images of differing scene type based on blur level within the images. We have chosen to study this sorting task for academic purposes.

Ten digitized, high-quality images were obtained from professional stock photography. These images represented five different scene types: birds, text, human faces, buildings, and landscapes. Four degrees of degradation for each of these images were then created by introducing increasing amounts of computer-generated Gaussian blur. This produced a data set of fifty pictures at five distinct blur levels, which are described by the adjectives "very good," "good," "fair," "poor," and "very poor."

The digitally simulated ring-wedge data for each of the images in the data set were subdivided into training and testing sets. A standard feed-forward neural network trained using the back propagation paradigm was chosen. This network had 32 ring-data input neurons, 32 wedge-data input neurons, 20 hidden neurons, and 5 output neurons corresponding to the five blur levels. The network was trained and tested. Tables 1(a)-2(b) show the recognition results from two different training-testing strategies. The first strategy, detailed in Table 1a, includes a

| Image Type | Learning | Test |
|---|---|---|
| Bird | A | B |
| IEEE Chart | A | B |
| Face | A | B |
| Building | A | B |
| Landscape | A | B |

(a)

| Blur Level | errors | recognition |
|---|---|---|
| very good | 0 | 100% |
| good | 0 | 100% |
| fair | 1 | 80% |
| poor | 1 | 80% |
| very poor | 1 | 80% |

(b)

*Table 1. (a) Training-testing strategy for an experiment based on blur-level recognition. Each letter symbol represents an original and the four corresponding degraded versions of that original. (b) Recognition results detailing error occurrences and correct recognition percentage*

| Image Type | Learning | Test |
|---|---|---|
| Bird | A | B |
| IEEE Chart | A | B |
| Face | | A, B |
| Building | A | B |
| Landscape | | A, B |

(a)

| Blur Level | errors | recognition |
|---|---|---|
| very good | 0 | 100% |
| good | 0 | 100% |
| fair | 1 | 86% |
| poor | 2 | 71% |
| very poor | 1 | 86% |

(b)

*Table 2. (a) Training-testing strategy for an experiment based on blur-level recognition. Each letter symbol represents an original and the four corresponding degraded versions of that original. (b) Recognition results detailing error occurrences and correct recognition percentage.*

representative from each scene type in both the learning and the testing sets. After training with this strategy, the neural network was able to recognize the blur level of the images in the testing set with the exception of three errors. The occurrence of these errors and the percentage of correct assessments for each blur level are presented in Table 1b. The second strategy, detailed in Table 2a, includes only three of the five scene types in the learning set and all five types in the testing set. After training with this strategy, the neural network was able to recognize the blur level of the images in the testing set with the exception of four errors. The occurrence of these errors and the percentage of correct assessments for each blur level are presented in Table 2b.

### Sorting Degradation Produced by Lossy Compression

As another aspect of our research, we wish to examine the effects of lossy image compression on the perceived quality of images. A preliminary experiment was conducted using a data set provided by the Eastman Kodak Company based on retrieval of images from several different compression routines and accompanied by a visual quality ratings made by trained photointerpreters.

As in the previous experiment, the digitally simulated ring-wedge data for each of the images in the data set were subdivided into training and testing sets, and a standard

feed-forward neural network trained using the back-propagation paradigm was again chosen. This network had 32 ring-data input neurons, 32 wedge-data input neurons, 20 hidden neurons, and 6 output neurons corresponding to 6 equidistant points on the scale used for the visual ratings of the images, which ranged for zero to five. The network was trained and tested. The results from the testing set showed a correlation between the automatic assessments and the human assessments of 0.92.

## Summary

The preliminary experiments presented in this report show encouraging results. Using digitally simulated diffraction pattern sampling in combination with neural network software, we have been able to rate images based on the amount of blur added to the image and the amount of degradation produced by lossy compression routines. As a result, each of these experiments is currently being re performed using larger data bases containing five hundred or more images. It is our hope that these and other experiments will show that for certain tasks automated image quality assessment will be capable of performing at the level of human assessment.

## Acknowledgment

The authors gratefully acknowledge helpful discussions with Rulon Simmons of the Eastman Kodak Company.

## References

1. A.J. Roufs, "Perceptual image quality: concept and measurement" *Philips J. Res.* 47(1), 35-62 (1992).
2. T.A. Grogan and D. Keene, "Image quality evaluation with a contour-based perceptual model," in *Human Vision, Visual Processing and Digital Display III*. Proc. SPIE, Vol. 1666, 188-97 (1992).
3. N.B. Nill and B.H. Bouzas, "Objective image quality measure derived from digital image power spectra," *Opt. Eng.* 31(4), 813-25 (1992).
4. J.A. Saghri, P.S. Cheatham, and A. Habibi "Image quality measure based on a human visual system model," *Opt. Eng.* 28(7), 813-18 (1989).
5. I.R.L. Davies, D. Rose, and R.J. Smith, "Automated image quality assessment," in *Human Vision, Visual Processing and Digital Display IV*, Proc. SPIE, Vol. 1913, 27-36 (1993).
6. N. George, J.T. Thomasson, and A. Spindel, "Photodetector Light Pattern Detector,: U.S. Patent No 3, 689,772, 5 September 1972.
7. N. Jensen, "High-speed image analysis techniques," *Photogrammetric Engineering*, 39, 1321-1328 (1973).
8. D.L. Venable, *Pattern Classification using Diffraction Pattern Sampling and the Limitations Due to Film Grain Noise*, Ph.D Thesis, University of Rochester, May 1989.
9. N. George, S. Wang, and D.L. Venable, "Pattern recognition using the ring-wedge detector and neural-network software," in *Optical Pattern Recognition II*, Proc SPIE, Vol 1134 96-106 (1989).
10. N. George and S. Wang, "Neural networks applied to diffraction pattern sampling," *Appl. Opt.*, 33 (1994).

# Controlled Blurring in Image Processing

*Bryan J. Stossel and Nicholas George*
*University of Rochester, Rochester, NY USA*

## Introduction

This paper reports some of the results of our research conducted in image processing with multiple-point impulse responses. The multiple point impulse response (MPIR) is defined as a number of impulses positioned within a prescribed region.[1] The results of this work have applications for imaging through turbulence, where this point-spread-function represents an idealized model of the atmosphere, and also image coding and transmission. This research provides information about the limits of real-time adaptive imaging imposed by the atmosphere.[2,3]

We will discuss the effects of blurring an intensity object scene with an MPIR and also show reconstructions obtained using an appropriate inverse filter. Also considered are some applications of this research to image coding and transmission.

## Blurring and reconstructions

The effect of the MPIR is to image a single impulse as, say, 25 to 200 irregularly positioned delta functions. A representative psf is shown in Fig. 1 where 25 points are placed within a 64x64 pixel window centered on the origin. This image has been enlarged by a factor of 2 in order to show clearly the impulses. Pictorially the effect of the MPIR on an object scene is as shown in Fig. 2. The blurred image is produced by convolution of the MPIR with an original scene consisting of 256x256 pixels with 8 bits/pixel. The resulting image is then quantized to 8 bits/pixel. As seen in Fig. 2, it appears visually as though the original scene is shrouded in fog, certainly it is blurred far beyond recognition. In theoretical terms it is readily shown that the power spectrum in the blurred image have been reshaped with the high frequency content being greatly reduced by the ratio 1/N, where N is the number of points in the MPIR.

An almost perfect image recovery is possible using an inverse filter generated from the two-dimensional spatial Fourier transform (FFT) of the degrading impulse response. Division of the FFT of the blurred object's intensity by the transfer function leads to an almost perfect recovery. It is surprising that a simple inverse filter is so effective, since in many other image recovery situations, contours of zeros in the transfer function lead to indeterminancies in the calculation of the recovered image. For the random-walk blur, we have shown that in general the FFT has only discrete zeros with the computational chance of encountering a zero thereby greatly reduced.

We will also discuss the artifacts introduced by several sources of error, using the artifact classification method of Tekalp and Sezan.[4] Included in the discussion are the effects of having incorrect magnitudes for the impulses in the psf used in the inverse filter as well as incorrectly positioning the impulses.

## Applications

Two interesting commercial applications of this research are being pursued. Since the high frequency detail is no longer apparent in the blurred image, it is reasonable to conjecture that FAX transmission of the images would require less space-bandwidth product than before. Using commercially available discrete-cosine-transform routines, we have found that it is much easier to transmit the blurred bird than the original. Estimates for improved transmission, reduced pixels, are from two to four times.

Secondly, transmission of the blurred object gives the sender a degree of privacy. With the widespread increase of FAX for color photographs, it is becoming increasing important to provide some degree of privacy in transmission, particularly for commercial art in advertising displays. Related experiments are presently being conducted for the coding and

transmission of engineering drawings and topographic maps.

This research is supported by the U. S. Army Research Office, the National Science Foundation, and the New York Science and Technology Foundation.

## References

1. B. Stossel and N. George, *Technical Digest, 1991 Opt. Soc. Amer. Annual Meeting, p.11, (1991)*
2. R. A. Muller and A. Buffington, *J. Opt. Soc. Amer.*, **64**: p. 1200 (1974)
3. D. L. Fried and J. L. Vaughn, *Appl. Opt.* **31** pp. 2865-2881 (1992)
4. A. M. Tekalp and M. I. Sezan, *Multidimensional Systems and Signal Processing*, 1, pp. 143-177 (1990)

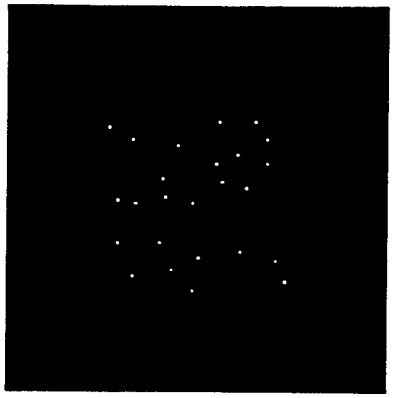

*Figure 1 MPIR consisting of 25 points, irregularly positioned within a 64x64 pixel window. The image has been enlarged by a factor of 2 for viewing purposes.*

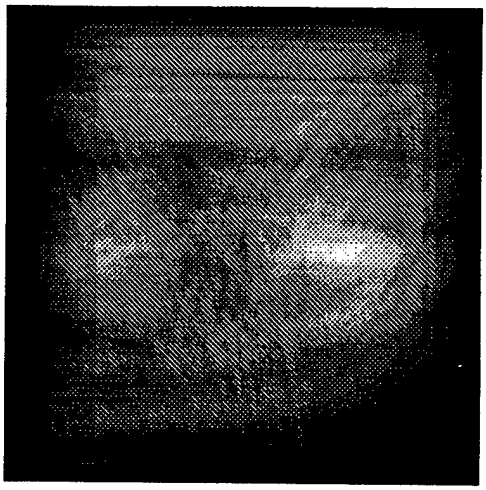

*Figure 2 Blurred image using the 25-point impulse response function corresponding to Fig. 1.*

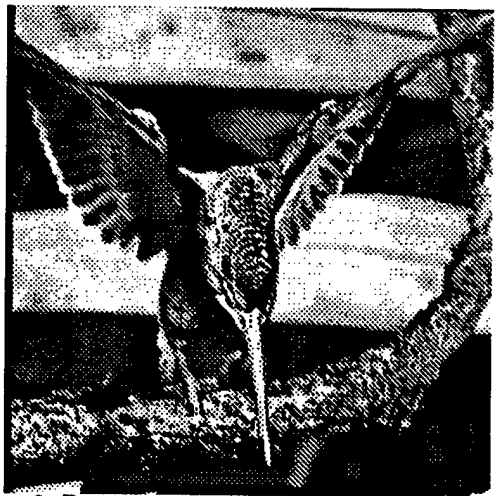

*Figure 3 Reconstructed image using an inverse filter corresponding the psf of Fig. 1. This image contains 256x256 pixels and is an excellent representation of the original scene.*

# Object Recognition and Image Coding

Nicholas George, B. J. Stossel, and D. M. Berfanger

Center for Electronic Imaging Systems (CEIS)
University of Rochester, Rochester, NY, 14627, USA

## INTRODUCTION

Research in electronic imaging is being conducted in a newly formed consortium in the Rochester community. The University of Rochester and the Rochester Institute of Technology have joined with leading corporations including Xerox, Eastman Kodak, 3M, Harris/RF Communications, and others in order to conduct cooperative research in electronic imaging. We have grouped the separate research into 9 major themes. In this presentation we will briefly review the scope of this Center's activity. Then, we will illustrate recent research results in two of the themes in more detail.

For object recognition, we describe an all-digital system that replaces the analog ring-wedge detector.[1] Other investigators have considered various hybrids: laser illumination with a CCD array in the transform plane and a software RW detector;[2] laser illumination and a holographic element to obtain RW-data format;[3] incoherent-to-coherent liquid crystal interface, laser illumination, holographic optical element to obtain RW-format;[4] and a RW-detector, laser illumination with a neural network for the classifier.[5] With respect to fingerprints important approaches are described in the literature.[6-10] A valuable source for neural network programming is the text by Masters.[11] Our main objective in this paper is to compare the performance of an all-digital RW-detector system with that of the analog multi-element array. To do this, we repeat and extend an earlier experiment.[12]

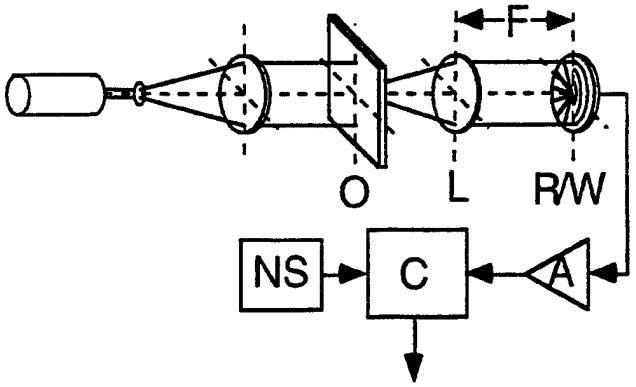


Fig. 1. Diffraction-pattern-sampling system incorporating the ring-wedge photodetector and neural-network software: O, input object; L, optical-transform lens; R/W, ring-wedge photodetector; NS, neural software; C, digital computer; A, amplifier and interface.

Invited paper presented and Takayanagi Memorial Session, Asia Display '95, Hamamatsu, Japan, October 1995.

## AUTOMATIC OBJECT RECOGNITION

### Fingerprint Recognition

In the literature excellent results have been reported for automatic recognition of thumbprints using the basic diffraction-pattern sampling setup shown in Fig. 1. From Ref. 12, we illustrate the data set, 8 thumbprints labeled F1 through F8. Using the analog ring-wedge detector and laser illumination, we reported an error of 1 in 160, see Table 1.1. In the present study our central objective is to establish the accuracy of an all-digital configuration, as shown in Fig. 2. It consists of an object (glass slide with thumbprint), a lens imaging to a CCD-array in white light, followed by the all-digital recognition module. For the image acquisition, it is important to recognize that fingerprints are rather complicated images, requiring approximately $4 \times 10^4$ pixels each for adequate representation.

### All-Digital Ring-Wedge Detector

For pattern recognition of an input image in white light, we would like to assert that the use of a ring-wedge detector array in the Fourier space of the intensity-based array image is a reasonable approach. With the intensity-based Fourier transform, we will demonstrate that both spatial spectral density and edge-content and edge-angle correlations are useful data forms for object recognition. Since the original RW-detector had 32 rings and 32 wedges based upon automating recognition in high resolution images in film,[1] we will use this as a basis for our all-digital RW-detector array. Hence, in Fig. 2, We have incorporated software appropriate for a

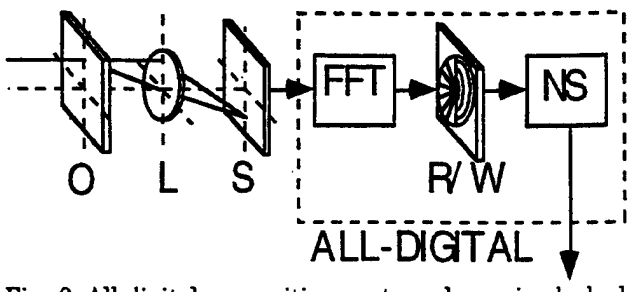


Fig. 2. All-digital recognition system shown in dashed box, including software embodiment for FFT, ring-wedge data format, and neural software.

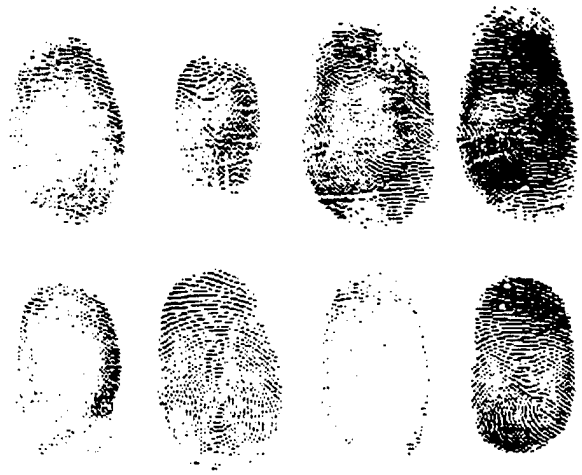

Fig. 3. Thumbprints used in thumbprint sorting experiments: F1 to F8, reading from left to right, top to bottom.

2-dimensional FFT followed by a software RW-detector module. There is data normalization followed by a neural network to perform the recognition.

In the experiment described in Ref. 12, the optical Fourier transforming system was set up such that the outer edge of the ring-wedge detector corresponded to a spatial frequency of 10.3 cycles/mm. Therefore, for the subsequent all-digital experiments described in the next section, digital images of all thumbprints in the data set were acquired using a scanning resolution of 20.6 samples/mm (8 bits/sample), corresponding to a Nyquist frequency of 10.3 cycles/mm. The sampling geometry of the digital system was then chosen to approximate closely the geometry of corresponding elements in the analog detector array.

## Recognition Experiments

Table 1.2 details the results of a sorting experiment using digital ring-wedge data calculated directly from the 8-bit-per-pixel, thumbprint images. As in the experiment described in Ref. 12, the data were separated into a learning set (5 each) and a testing set (20 each). In structuring the neural network we chose a three-layer, fully connected, feedforward configuration trained using a normalized cumulative backpropagation learning paradigm. The network had 59 input neurons (rings 6-32 and wedges 1-32), 12 hidden neurons, and 8 output neurons (F1-F8). Input data were preprocessed to be scaled approximately from -1 to +1. The logarithms of the ring data were used with an appropriate bias subtracted off and wedge data were rank ordered and normalized. We found an error rate of 2 in 160. Separately, we have been successful with ring-only (orientation-independent) and wedge-only (scale-independent) sortings.

| Table 1.1 | Maximum Valued Ouput Neuron | | | | | | | |
|---|---|---|---|---|---|---|---|---|
| Testing Set | 1 | 2 | 3 | 4 | 5 | 6 | 7 | 8 |
| F1 | 20 | | | | | | | |
| F2 | | 20 | | | | | | |
| F3 | | | 20 | | | | | |
| F4 | | | | 20 | | | | |
| F5 | | | | | 20 | | | |
| F6 | | | | 1 | | 19 | | |
| F7 | | | | | | | 20 | |
| F8 | | | | | | | | 20 |

| Table 1.2 | Maximum Valued Ouput Neuron | | | | | | | |
|---|---|---|---|---|---|---|---|---|
| Testing Set | 1 | 2 | 3 | 4 | 5 | 6 | 7 | 8 |
| F1 | 20 | | | | | | | |
| F2 | | 19 | | | | | | 1 |
| F3 | | | 20 | | | | | |
| F4 | | | | 20 | | | | |
| F5 | | | | | 20 | | | |
| F6 | | | | | | 19 | | 1 |
| F7 | | | | | | | 20 | |
| F8 | | | | | | | | 20 |

| Table 1.3 | Maximum Valued Ouput Neuron | | | | | | | |
|---|---|---|---|---|---|---|---|---|
| Testing Set | 1 | 2 | 3 | 4 | 5 | 6 | 7 | 8 |
| F1 | 20 | | | | | | | |
| F2 | | 20 | | | | | | |
| F3 | | | 20 | | | | | |
| F4 | | | | 20 | | | | |
| F5 | | | | | 20 | | | |
| F6 | | | | | | 20 | | |
| F7 | | | | | | | 20 | |
| F8 | | | | | | | | 20 |

| Table 1.4 | Maximum Valued Ouput Neuron | | | | | | | |
|---|---|---|---|---|---|---|---|---|
| Testing Set | 1 | 2 | 3 | 4 | 5 | 6 | 7 | 8 |
| F1 | 20 | | | | | | | |
| F2 | | 20 | | | | | | |
| F3 | | | 20 | | | | | |
| F4 | | | | 20 | | | | |
| F5 | | | | | 20 | | | |
| F6 | | | | | | 20 | | |
| F7 | | | | | | | 20 | |
| F8 | | | | | | | | 20 |

Table 1.3 details the results from a sorting experiment using digital ring-wedge data calculated from binary images of the fingerprints obtained by globally thresholding each image at its mean gray level value. When the same learning/testing strategy, network structure, and input preprocessing were utilized, as described above, we found zero errors in 160.

Table 1.4 details the results from a sorting experiment using digital ring-wedge data calculated from only the odd part of the binary images used previously. The same learning/testing strategy, network structure, and input preprocessing were utilized, as described above. Again, we found zero errors in 160. A similar experiment using only the even part of the binary images also resulted with zero errors in 160. The use of even-part, odd-part, and phase features of the all-digital system presents important new possibilities which we are investigating.

## IMAGE BLUR FOR CODING

### Image Restoration and the MPIR

Image restoration for scenes that have been degraded by a multiple-point impulse response (MPIR) has been studied recently[13-15]. The multiple-point impulse response is prescribed to be a number of impulses positioned within a specified region. The MPIR provides a particularly interesting case of blurring that lends itself to theoretical calculations such as the filtering properties of the transfer function and the average number of zeros per area of the transfer function. This impulse response also has interesting applications for image coding and compression

Our central interest is the recovery of intensity images that have been blurred by a multiple-point impulse response, $b(x,y)$ that consists of a number, N, of irregularly positioned impulses defined by

$$b(x,y) = \sum_{n=1}^{N} \delta(x - x_n, y - y_n), \qquad (1)$$

where $\delta(x,y)$ is the two-dimensional Dirac delta function and $(x_n,y_n)$ are the positions of the impulses as in Fig. 4. The transfer function corresponding to this multiple-point blur function is

$$B(u,v) = \sum_{n=1}^{N} \exp\left[-i2\pi(ux_n + vy_n)\right], \qquad (2)$$

where $i^2=-1$. One notices immediately the random-walk nature of this transfer function.

We now present the results of blurring an original scene with an MPIR of the form given by Eq. (1) as well as reconstruction results using a generalized inverse-filter algorithm. The MPIR, shown in Fig. 4, consists of 50 unit amplitude impulses uniformly distributed within a 64x64 pixel region, centered on the origin. The original 8 bits/pixel object scene is blurred by the MPIR and quantized to 8 bits/pixel, thus introducing quantization noise. The blurred image is shown in Fig. 5. The original object scene has been zero-padded to eliminate truncation artifacts[16]. One can see from this figure that the 50-point impulse response has obscured the fine details of the image and that the original object is no longer distinguishable. The recovered image shown in Fig. 6 is an excellent representation of the original object. Similarly good reconstructions are obtained for 25 impulses within the same 64x64 pixel window, as well as for 100 and 200 impulses.

The excellent results obtained in Fig. 6 are due to the fact that the zeros of the random-walk transfer function $B(u,v)$ occur at isolated frequencies. We have derived a theoretical expression for the average number of zeros per area present in the transfer function based on previous work on the zeros of speckle patterns.[13,14,17]

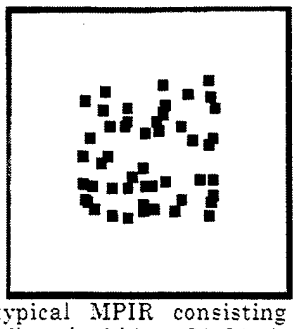

Fig. 4 A typical MPIR consisting of 50 impulses uniformly distributed within a 64x64 pixel window.

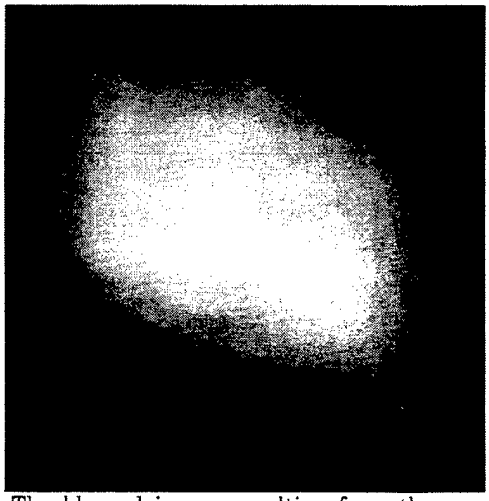

Fig. 5 The blurred image resulting from the convolution of the impulse response of Fig. 4 and the original scene. The original scene is obscured within this image.

Fig. 6 The restored original scene using a generalized inverse filter algorithm. Note the high frequency details of the rotunda and flag pole.

### Filtering properties of the MPIR

An important aspect of the MPIR and the corresponding random-walk transfer function is its filtering properties. A convenient measure of the frequency response of the system is the average power spectrum, $\langle B(u,v)B^*(u,v)\rangle$ where the asterisk represents the complex conjugate and

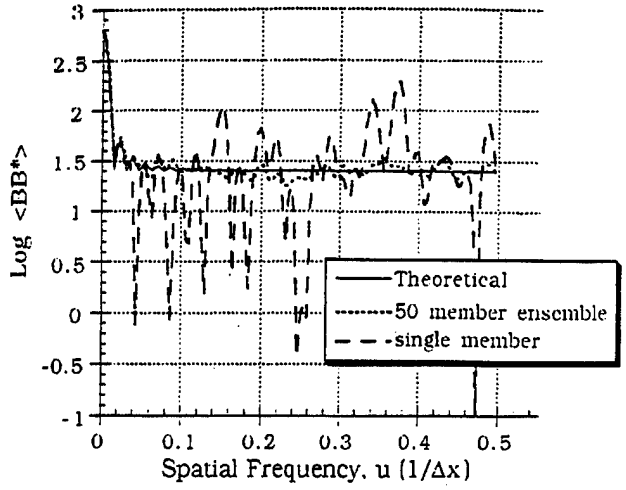


Fig. 7 Plot of the average power spectrum for the case where 50 impulses are uniformly distributed within a 64x64 window.

the ensemble average is over an ensemble of different realizations of $x_n$ and $y_n$. Substitution of Eq. (2) into the average power spectrum yields

$$\langle B(u,v)B^*(u,v)\rangle = \left\langle \sum_{m=1}^{N} \exp\left[-i2\pi(ux_m + vy_m)\right] \times \sum_{n=1}^{N} \exp\left[i2\pi(ux_n + vy_n)\right] \right\rangle. \quad (4)$$

Omitting the details of the statistical calculation[13], we can evaluate Eq. (4) based on the assumptions that $x_n$ and $y_n$ are independent, uniformly distributed random processes within a window $W_x x W_y$. The resulting expected value for the power spectrum is found to be

$$\langle B(u,v)B^*(u,v)\rangle_{uniform} = N + (N^2 - N)\,\mathrm{sinc}^2(uW_x)\,\mathrm{sinc}^2(vW_y). \quad (5)$$

From Eq. (5) it can be seen that the high spatial frequencies are attenuated by a factor of $1/N$ with respect to the dc value. These characteristics can be seen in Fig. 7 which contains a plot of the average power spectrum when $W_x$=$W_y$=64. Shown in the plot are three curves: the theoretical curve corresponding to Eq. (5), an experimental curve for an ensemble of 50 members, and an experimental curve for a single realization.

## Image compression and noise

The controlled image blur, as in Fig. 5, is well suited to efficient and private data transmission and we describe the use of DPCM and DCT-based algorithms. For DPCM compression, we find that the bit rates required in a Huffman code can be reduced up to 50% by using a multiple-point blur prefilter. Correspondingly we find a reduction of 70% in the bit rate for the DCT-based case, over using DCT with the original image. It is found that practical bit rates on the order of one bit per pixel can be achieved with excellent quality. We find, too, that controlled blurring is useful in transmitting images that are immersed in speckle, using the simple test target shown in Fig. 8[18]. Controlled blurring provides a useful means of coding a speckled image for efficient transmission and recovery. This technique is expected to be of value in the transmission of ultrasound images. This research was supported in part by the U.S. Army Research Office and by the National Science Foundation.

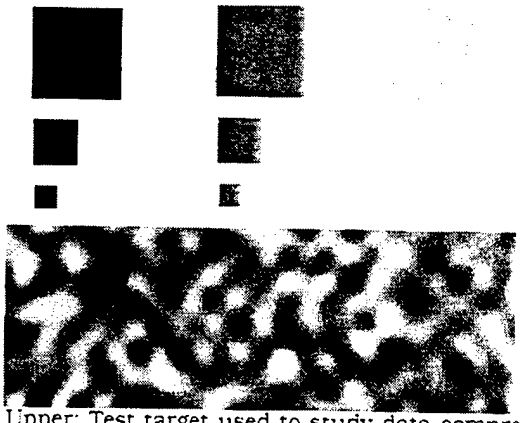

Fig. 8 Upper: Test target used to study data compression algorithms on images corrupted by speckle noise. Lower: Typical speckle noise where the average speckle size is on the order of the smallest test target object.

**References**


1. N. George, J. T. Thomasson, and A. Spindel, "Photodetector light pattern detector," U.S. patent 3,689,772 (5 September 1972).
2. R. K. O'Toole and H. Stark, Appl. Opt. **19**, 2496-2506 (1980).
3. M. S. Brown, Optica Acta **31**, 507-513 (1984).
4. D. Clark and D. P. Casasent, Opt. Eng. **27**, 365-371 (1988).
5. N. George, S. G. Wang, and D. L. Venable, Proc. Soc. Photo-Opt. Instrum. Eng. **1134**, 96-106 (1989).
6. H. Matsumoto, S. Narita, M. Ishii, A. Nishiyamma, N. Senuma, H. Hohmi, K. Kiji, Y. Hoshino, K. Asai, and K. Shoha, NEC Res. Dev. (Japan) **96**, 143-159 (1990).
7. M. Kamijo, H. Mieno, and K. Kojima, Syst. Comput. Jpn. (USA) **23**, 89-101 (1992).
8. Y. He, R. Kohno, and H. Imai, IEICE Transactions on Fundamentals of Electronics, Communications and Computer Sciences, **E76-A**, 1469-1482 (1993).
9. M. O. Freeman, A. Fedor, B. Bock and K. Duell, Proc. Soc. Photo-Opt. Instrum. Eng. **1772**, 241-250 (1992).
10. J. Ohta, J. Sharpe, K. Johnson, Opt. Comm. **111**, 451-458 (1994).
11. T. Masters, *Practical Neural Network Recipes in C++* (Academic Press, Inc., New York, 1993).
12. N. George and S. G. Wang, App. Opt. **33**, 3127-3134 (1994).
13. B.J. Stossel, Ph.D. thesis, Univ. Rochester, Rochester, NY (1994)
14. N. George and B.J. Stossel, patent application granted, Serial No. 08/154311 (Filed 1993)
15. B.J. Stossel and N. George, Optics Comm., Oct. (1995)
16. M. I. Sezan and A. M. Tekalp, IEEE Trans. Acoust. , Speech, Signal Proc., **38**, 181-185 (1990)
17. N.B. Baranova and B. Ya. Zel'dovich, Sov. Phys. JETP **53**, 925-929 (1981)
18. N. George, C.R. Christensen, J.S. Bennett, and B. Guenther, J. Opt. Soc. Am. **66**, 1282-1290 (1976).

ELSEVIER

1 January 1996

OPTICS COMMUNICATIONS

Optics Communications 122 (1996) 212

Erratum

# Multiple-point impulse responses: controlled blurring and recovery (Optics Comm. 121 (1995) 156)

Bryan J. Stossel, Nicholas George

*The Institute of Optics, University of Rochester, Rochester, NY 14627, USA*

Due to an oversight of the publisher two figures on p. 158 of the paper are interchanged. The correct figures with their captions are as follows:

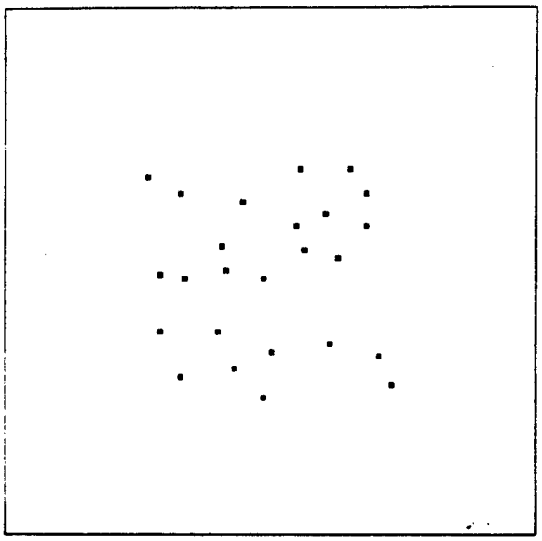

Fig. 1. MPIR consisting of 25 points, irregularly positioned within a 64 x 64 pixel window. The image has been enlarged and the grey levels inverted (black = 255) to show detail.

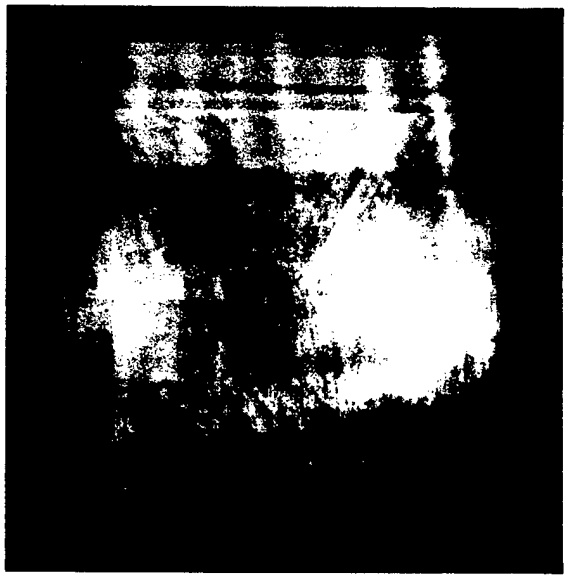

Fig. 2. Blurred image using the 25-point impulse response function shown in Fig. 1. The original scene contains 256 x 256 pixels.


*SSDI* 0030-4018(95)00705-9

ELSEVIER

1 December 1995

OPTICS COMMUNICATIONS

Optics Communications 121 (1995) 156–165

*Full length article*

# Multiple-point impulse responses: controlled blurring and recovery ☆

Bryan J. Stossel, Nicholas George

*The Institute of Optics, University of Rochester, Rochester, NY 14627, USA*

Received 12 April 1995; revised version received 10 July 1995

**Abstract**

We present the results of controlled blurring of an image using a multiple-point impulse response and thereafter recovering the original scene using a generalized inverse filter. The multiple-point impulse response consists of delta-function impulses irregularly positioned within a prescribed area. This impulse response is shown to degrade the image beyond recognition. Excellent recoveries are obtained for pictorial and textural images. An important result is that the zeros of the transfer function occur at discrete locations and therefore have a negligible effect on the image recovery using the generalized inverse filter.

## 1. Introduction

Several aspects of image restoration for scenes that have been degraded by a multiple-point impulse response (MPIR) are presented. The multiple-point impulse response is prescribed to be a number of impulses positioned within a specified region. This impulse response provides a particularly interesting case of blurring that lends itself to theoretical calculations, and hence leads to a better understanding of the limits imposed on image recovery. In this paper our interest is the use of the MPIR to blur an object scene in a controlled manner. Such an application reduces the amount of high frequency detail in the image and can render the original scene unrecognizable to an observer. We believe that study of this highly idealized impulse response may have importance in image compression and may provide insight into image recovery for images degraded by propagation through a turbulent medium.

Early image restoration using inverse filtering and computer methods are described by Harris [1]. The extension to optical processing in the presence of noise [2] and a comprehensive listing of various image restoration methodologies [3] have been published. In this early work attention was directed toward the deleterious effects of contours of zeros in the blur transfer function. These zero contours inhibit the use of the inverse filter in most practical applications. A significant result presented here is that essentially complete image recovery is possible for blurring due to MPIR degradations using a generalized inverse filter. As described herein, the excellent reconstructions are possible, in large part, because the zeros of the transfer function occur at discrete locations and thus are rarely encountered in sampling with the generalized inverse filter. We show that the theoretical expression for the average number of zeros in the transform space is confirmed by computer simulation.

In this paper we present in Sec. 2 a description of the imaging model including the functional form of the impulse response and the corresponding transfer func-

☆ This research is supported in part by the U.S. Army Research Office, the National Science Foundation, and the New York State Science and Technology Foundation.


*SSDI* 0030-4018(95)00460-2

tion. In Sec. 3 results are presented for the blurring process as well as the recovery of a pictorial image that has been blurred by a 25-point impulse response. It is shown that, provided the positions of the impulses are known precisely, excellent reconstructions are obtained. The discrete nature of the zeros in the transfer function is demonstrated in Sec. 4 as well as the outline of a theoretical calculation of the average number of zeros per area of the random-walk transfer function corresponding to the MPIR. A plot of the average number of zeros per area, comparing the theoretical calculation and experimental results, is presented for the case where the impulses are uniformly distributed within a square window [4,5]. The results presented in Sec. 5 for the coding and decoding of a textual image blurred by a 50-point impulse response illustrate that the fact that the MPIR may be used to obscure an image beyond recognition and that with knowledge of the coding key the original data may be recovered.

## 2. Multiple-point impulse response functions

Consider an object having an intensity described by the function $f(x, y)$ where $(x, y)$ are the spatial coordinates. This scene is blurred in a controlled manner by convolution with a blurring function $b(x, y)$, also known as the point spread function (psf). The intensity of the blurred image $g(x, y)$ for a linear system is given by

$$g(x, y) = f(x, y) * b(x, y) + n(x, y) , \qquad (1)$$

where the asterisk, $*$, represents the two-dimensional convolution operator and $n(x, y)$ is an additive noise term.

By taking the Fourier transform of Eq. (1), the spatial-frequency representation for the blurred image is given by

$$G(u, v) = F(u, v)B(u, v) + N(u, v) , \qquad (2)$$

where upper case functions represent the two-dimensional, spatial, Fourier transforms of their lower case counterparts, and $(u, v)$ are the spatial frequency coordinates corresponding to the spatial coordinates $(x, y)$ respectively. $B(u, v)$ is the transfer function for the system. The image recovery problem is then to obtain a reasonable estimate, $\hat{f}(x, y)$, of the original scene $f(x, y)$ given $g(x, y)$, the observed image, and $\hat{b}(x, y)$, an estimate of the blur function $b(x, y)$. Herein the caret ($\hat{}$) is used to designate an estimate of the named function. Errors between the original object $f(x, y)$ and the recovered estimate $\hat{f}(x, y)$ may arise from several sources [6]. The sources of error of most interest to us regarding the MPIR are errors made in the determination of the point spread function, $b(x, y)$, as well as errors due to those regions in the transform domain where the recorded image spectrum is zero. The artifacts introduced by these errors have been studied [4] and will be reported in a separate publication.

Our central interest is the recovery of intensity images that have been blurred by a system characterized by a multiple-point impulse response, $b(x, y)$. This impulse response consists of a number, $N$, of irregularly positioned impulses and is defined by

$$b(x, y) = \sum_{n=1}^{N} a_n \delta(x - x_n, y - y_n) , \qquad (3)$$

where $\delta(x, y)$ is the two-dimensional Dirac delta function [7]. This particular blur function represents a set of $N$ impulses with amplitudes $a_n$ and positions $(x_n, y_n)$. The transfer function corresponding to this multiple-point blur function is

$$B(u, v) = \sum_{n=1}^{N} a_n \exp[-i2\pi(ux_n + vy_n)] , \qquad (4)$$

where $i^2 = -1$. One notices immediately the random-walk nature of this transfer function. We may consider the transfer function at spatial-frequency coordinate $(u, v)$ to be comprised of a sum of $N$ complex phasors with the amplitude of the $n$th phasor being $a_n$ and its phase angle $2\pi(ux_n + vy_n)$.

## 3. Image degradation and recovery

We now present the results of blurring an original scene with an MPIR of the form given by Eq. (3) as well as reconstruction results using a generalized inverse filter algorithm. The MPIR, shown in Fig. 1, consists of 25 unit amplitude impulses positioned within a $64 \times 64$ pixel region, centered on the origin. The positions of the impulses are chosen from a computer generated ensemble of uniformly distributed random numbers. The original 8 bits/pixel object scene is blurred by the MPIR and quantized to 8 bits/pixel, thus

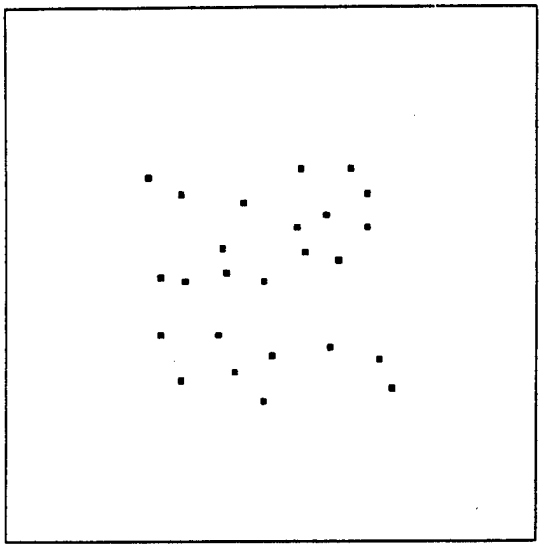

Fig. 1. MPIR consisting of 25 points, irregularly positioned within a 64×64 pixel window. The image has been enlarged and the grey levels inverted (black = 255) to show detail.

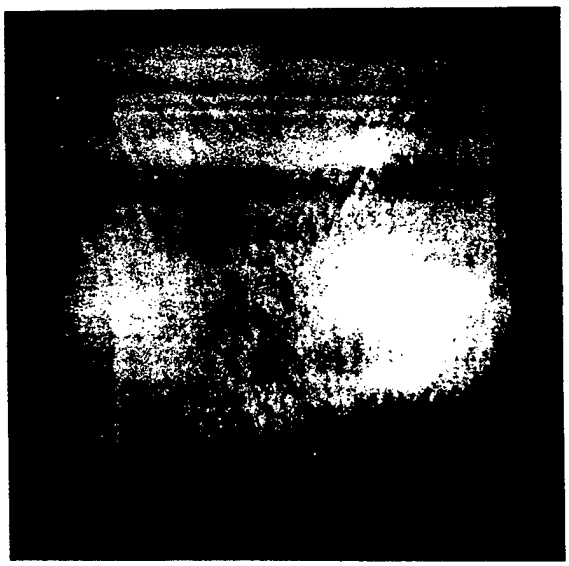

Fig. 2. Blurred image using the 25-point impulse response function shown in Fig. 1. The original scene contains 256×256 pixels.

introducing quantization noise. It has been found for the MPIR that quantization results in noise that is approximately 20dB below the signal. The blurred image is shown in Fig. 2. The original object scene has been zero-padded to eliminate truncation artifacts [6], which would result if the blurred image was restricted to the same number of pixels as the original scene. One can see from this figure that the 25-point impulse response has obscured the fine details of the image and that the original object is no longer distinguishable. The recovered image shown in Fig. 3 is an excellent representation of the original object, having an rms error of approximately two percent. Similarly good reconstructions are obtained for 50 impulses within the same 64×64 pixel window, as well as for 100 and 200 impulses.

The method used to recover the object scene is a generalized inverse filter where the filter operator $P(u, v)$ is described by

$$P(u, v)G(u, v) = \begin{cases} \dfrac{G(u, v)}{\hat{B}(u, v)}, & \hat{B}(u, v) \neq 0, \\ 0, & \hat{B}(u, v) = 0, \end{cases} \tag{5}$$

where $\hat{B}(u, v)$ is an estimate of the spatial Fourier transform of the blur function. It is well known that the direct solution of Eq. (2) leads to an ill-posed problem and thus some means of regularization must be incorporated [8,9]. It is also clear that the filter described by Eq. (5) is only weakly regularized. Due to the small

Fig. 3. Reconstructed image using a generalized inverse filter corresponding to the psf of Fig. 1 and defined in Eq. (5). This scene contains 256×256 pixels.

values of $B(u, v)$, any errors in determining either $G(u, v)$ or $B(u, v)$ in the neighborhood of a zero become greatly amplified resulting in the so-called data-discontinuity problem where small perturbations in the data result in large errors in the reconstruction. This problem is particularly important when the zeros of the transfer function form continuous contours [6] and thus few problems can be solved using such an algorithm.

Before turning to a discussion of the zeros of the random-walk transfer function and a practical application of the MPIR, let us illustrate, using two common examples for $b(x, y)$, the typical deleterious effects of encountering zeros and small values in the transfer function when using the inverse filter. While no doubt well-known to researchers in the field, the image retrieval is so poor in a typical case that it is difficult to find illustrative examples in the literature. In the paragraphs below we present the recovery results for a square impulse response and a Gaussian blur using the generalized inverse filter of Eq. (5).

The case for which $b(x, y)$ is a square blur function yields a transfer function given by

$$B(u, v) = \frac{\sin(\pi L_x u)}{\pi u} \frac{\sin(\pi L_y v)}{\pi v}, \tag{6}$$

which contains zeros for $u = m/L_x$ and $v = n/L_y$, where $m$ and $n$ are integers. Shown in Figs. 4a and 4b are the degraded and restored images for the case where the blur function is a $6 \times 6$ square. The noise amplification due to the small values of the transfer function in the neighborhood of the zero contours is clearly seen as strong periodic artifacts in the recovered image. A more subtle illustration of the need for regularization is given by the case when the impulse response is a Gaussian. Shown in Figs. 4c and 4d are the degraded and restored images when the blur function is a Gaussian with a standard deviation of 5 pixels. In this case the transfer function has no zeros, and yet even for this relatively small amount of degradation the generalized inverse-filter result in Fig. 4d is dominated by noise and is markedly poorer than the original degraded scene.

It is clear from Figs. 4a and 4c that the amount of visual degradation introduced by the square and Gaussian psfs is considerably less than for the case of the 25-point MPIR. The reconstructions shown in Figs. 3, 4b, and 4d accentuate the excellent results obtained for the MPIR, and serve to delineate the remarkable ability of the generalized inverse filter to recover the original scene for multiple-point impulse response degradations. They also illustrate the importance of understanding the structure of the zeros in the transfer function and the role the zeros have in the application of reconstruction algorithms.

## 4. Zeros of the transfer function

An important property of the random-walk transfer function is that the zeros occur at discrete spatial frequencies. This property is illustrated in Figs. 5 and 6. The zero contours for the real and imaginary parts of the transfer function are shown in Figs. 5a and 5b respectively. It is obvious that the zero contours form closed, continuous curves as is expected for the intersection of the three-dimensional surfaces $R(u, v)$ and $X(u, v)$ with the zero-plane. On the other hand, the zeros of the transfer function occur at the intersection points of these two sets of curves. The zeros of the transfer function are shown in Fig. 6a, with an enlarged view of the inset shown in Fig. 6b. From Figs. 6a and 6b, it is seen that the zeros of the transfer function do indeed occur at discrete points.

Since the zeros of the transfer function are discrete, they are countable. Isolated zeros have been reported in the literature on crystallography [10,11] and acoustics [12], and there has been important consideration of isolated zeros in speckle patterns, [13,14]. However calculation of the average number of zeros per area for the specific case of the zeros of the random walk of Eq. (3) has not been found. Herein we present the essential details of this calculation.

As seen from Eq. (3), the transfer function $B(u, v)$ is in general a complex function which can be rewritten as

$$B(u, v) = R(u, v) + \mathrm{i}X(u, v), \tag{7}$$

where $R(u, v)$ and $X(u, v)$ are the real and imaginary parts of the transfer function respectively. Baranova et al. [13] have presented an interesting expression for the average number of zeros per area, $M$, of a complex function, which in a suitable form is given by

$$M_{\mathscr{A}} = \left\langle \int_{\mathscr{A}} \delta[R(u, v)]\ \delta[X(u, v)]\ \mathrm{d}R\ \mathrm{d}X \right\rangle, \tag{8}$$

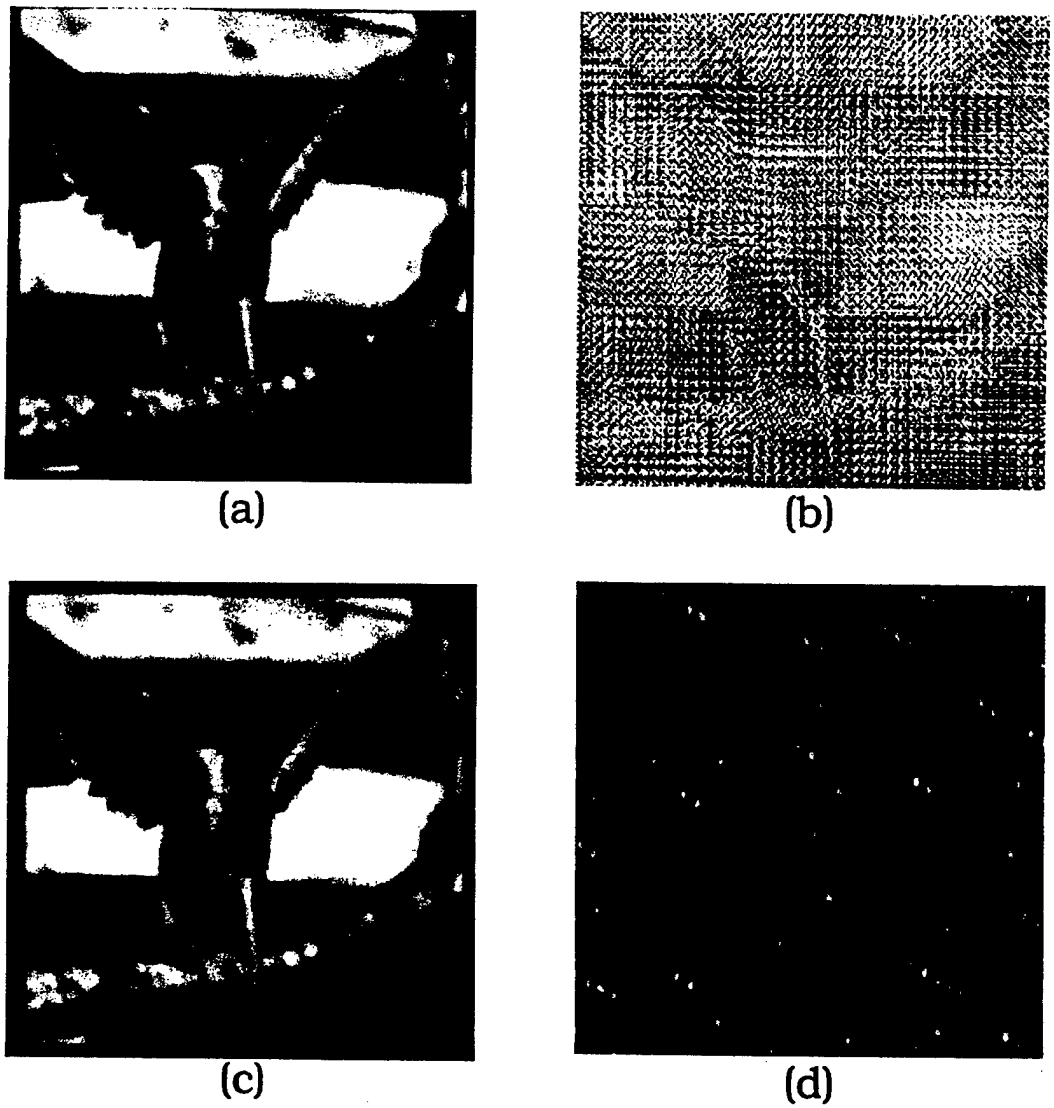


Fig. 4. Blurred and recovered images for common psfs using the generalized inverse filter. (a) The degraded image using a 6×6 pixel square psf. (b) The generalized inverse filter result for (a). (c) The degraded image using a Gaussian psf with a 4-pixel standard deviation. (d) The generalized inverse filter result for (b).

where the integral is taken over a prescribed area $\mathscr{A}$. The bracket notation $\langle \ldots \rangle$ is used to denote an average over an ensemble of realizations. This expression can be seen to count the number of zeros in the transfer function, since the integrand is nonzero only when both the real and imaginary parts of the transfer function are simultaneously zero, in which case the value of $M\mathscr{A}$ is incremented by one. After making a change of variables from $R$ and $X$ to the real variables $u$ and $v$ and applying the definition of ensemble average, Eq. (8) can be written as

$$M\mathscr{A} = \int \ldots \int \delta[R(u, v)]\ \delta[X(u, v)]\ |J| \times p_6(R, X, R_u, R_v, X_u, X_v) \times dR\ dX\ dR_u\ dR_v\ dX_u\ dX_v\ du\ dv\,. \quad (9)$$

In Eq. (9), $|J|$ is the transformation Jacobian,

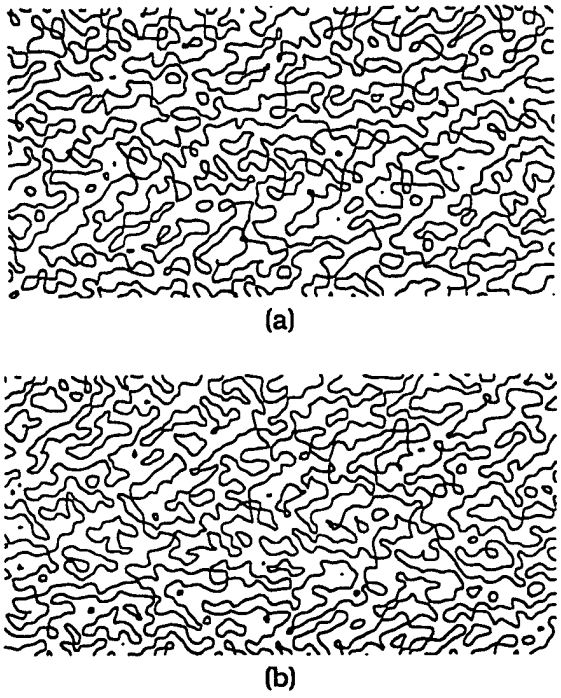


Fig. 5. (a) Zero-contour plot for the real part of a random-walk transfer function. Only the upper half-plane ($v \geq 0$) is shown. (b) Zero-contour plot for the imaginary part of the same random-walk transfer function as in (a). Again only the upper half-plane ($v \geq 0$) is shown. The real and imaginary parts are real-valued functions and the zero contours form continuous, closed curves.

$$R_u = \frac{\partial R}{\partial u}, \quad R_v = \frac{\partial R}{\partial v}, \quad X_u = \frac{\partial X}{\partial u}, \quad X_v = \frac{\partial X}{\partial v}, \quad (10)$$

and $p_6(\ldots)$ is the sixth order joint density function of the enclosed variables, $R$, $X$, $R_u$, $R_v$, $X_u$, and $X_v$. The notation $\int \ldots \int$ is used to represent all of the integrals corresponding to the differentials in the integrand taken over appropriate intervals. It is a straightforward exercise to reduce Eq. (9) to a one-dimensional form (dropping $X$ and $v$) and obtain a result equivalent to Rice's [15] result for the expected number of zeros of a random noise current.

In order to evaluate Eq. (9), an expression for the joint density function, $p_6(\ldots)$, is needed. The sixth order joint density function can be simplified to a product of first order density functions provided it can be shown that the fields and their first partial derivatives obey Gaussian statistics and are all mutually uncorrelated. It is well known that the statistics of the random-walk are asymptotically Gaussian [16–18]. For the case of a small number of scatterers (a small number of steps in the random-walk), it is known that the two-dimensional random walk does not obey Gaussian statistics [19–21]. The regime in which the statistics begin to become Gaussian has been found to be $N \approx 7$ [21,22]. It is readily found for typical cases, where $N \geq 20$, that the real and imaginary parts of the transfer function are well approximated by Gaussians [4]. The fact that the real and imaginary parts of the transfer function are Gaussian ensures that the first partial derivatives are also Gaussian [17].

If the field components can be shown to be mutually uncorrelated, then, since each component obeys Gaussian statistics, the sixth order joint density function may be simplified into the product of the first order density functions of each component. While the details of the derivation are not presented here, it can be shown that

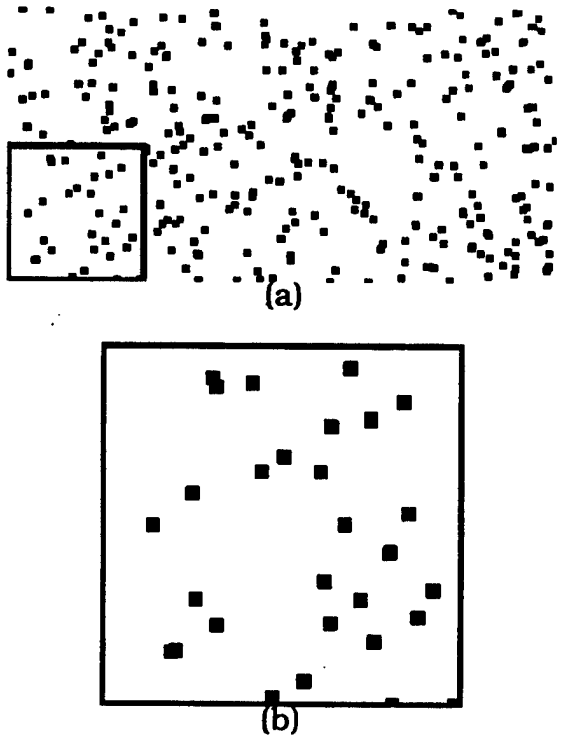


Fig. 6. (a) Zero-contour plot for the random-walk transfer function corresponding to Fig. 5a and 5b. Only the upper half-plane ($v \geq 0$) is shown. The transfer function is a complex-valued function and the zero contours are formed by the intersection of the two sets of continuous, closed curves shown in Fig. 5. The zeros occur at isolated points. (b) An exploded view of the inset region of (a).

all field components, $R(u, v)$, $X(u, v)$, $R_u(u, v)$, etc., are mutually uncorrelated provided the region of interest in the transform domain is restricted to those spatial frequencies where the characteristic function of the positions of the multiple-point impulses is negligible. It is also required that the impulses be distributed such that the 'center of mass' of the impulses is located at the origin. Under these assumptions, the sixth order joint density function is rewritten as

$$p_6(R, X, R_u, X_u, R_v, X_v) = p_R(R)p_X(X)p_{R_u}(R_u)p_{X_u}(X_u)p_{R_v}(R_v)p_{X_v}(X_v) , \tag{11}$$

where the notation $p_z(z)$ represents the first order Gaussian density function for the random variable $z$. Substituting appropriate expressions for the Gaussian density functions into Eq. (11) and the result into Eq. (9), the expression for the average number of zeros becomes

$$\begin{aligned} M\mathscr{A} = & \int \cdots \int \delta(R)\,\delta(X)\,|J| p_R(R)p_X(X) \\ & \times p_{R_u}(R_u)p_{X_u}(X_u)p_{R_v}(R_v)p_{X_v}(X_v) \\ & \times \mathrm{d}R\,\mathrm{d}X\,\mathrm{d}R_u\,\mathrm{d}R_v\,\mathrm{d}X_u\,\mathrm{d}X_v\,\mathrm{d}u\,\mathrm{d}v \\ = & \frac{1}{(2\pi)^3} \int \cdots \int \frac{\delta(R)\,\delta(X)\,|J|}{\sigma_R\sigma_{R_u}\sigma_{R_v}\sigma_X\sigma_{X_u}\sigma_{X_v}} \\ & \times \exp\left[ -\frac{(R-\mu_R)^2}{2\sigma_R^2} - \frac{(X-\mu_X)^2}{2\sigma_X^2} \right] \\ & \times \exp\left[ -\frac{(R_u-\mu_{R_u})^2}{2\sigma_{R_u}^2} - \frac{(X_u-\mu_{X_u})^2}{2\sigma_{X_u}^2} \right] \\ & \times \exp\left[ -\frac{(R_v-\mu_{R_v})^2}{2\sigma_{R_v}^2} - \frac{(X_v-\mu_{X_v})^2}{2\sigma_{X_v}^2} \right] \\ & \times \mathrm{d}R \ldots \mathrm{d}X_v\,\mathrm{d}u\,\mathrm{d}v , \end{aligned} \tag{12}$$

where it is not assumed that the field components are zero-mean and the spatial-frequency dependence of the variances $\sigma_R$, $\sigma_X$, $\sigma_{R_u}$, etc., has been retained, although not explicitly shown. Satisfying the conditions for which the field components are uncorrelated also assures that each component is in fact zero-mean, the variances are independent of the spatial frequencies $u$ and $v$, and $\sigma_R = \sigma_X$, $\sigma_{R_u} = \sigma_{X_u}$, and $\sigma_{R_v} = \sigma_{X_v}$. Therefore the average number of zeros may be written as

$$\begin{aligned} M\mathscr{A} = & \frac{1}{(2\pi)^3\sigma_R^2\sigma_{R_u}^2\sigma_{R_v}^2} \int \cdots \int \delta(R)\,\delta(X)\,|J| \\ & \times \exp\left[ -\left( \frac{R^2+X^2}{2\sigma_R^2} \right) \right] \\ & \times \exp\left[ -\left( \frac{R_u^2+X_u^2}{2\sigma_{R_u}^2} + \frac{R_v^2+X_v^2}{2\sigma_{R_v}^2} \right) \right] \\ & \times \mathrm{d}R\,\mathrm{d}X\,\mathrm{d}R_u\,\mathrm{d}R_v\,\mathrm{d}X_u\,\mathrm{d}X_v\,\mathrm{d}u\,\mathrm{d}v . \end{aligned} \tag{13}$$

It is noted that we have made the assumption that either the characteristic function for the impulse positions is delta-like or that we are restricting the range of integration to those frequencies for which the characteristic function is negligible.

Eq. (13) is readily evaluated to give

$$M = \frac{\sigma_{R_u}\sigma_{R_v}}{2\pi\sigma_R^2} , \tag{14}$$

for the average number of zeros per area. In those regions of the transform domain where the characteristic functions of the positions of the impulses are negligible, the variances are given as

$$\sigma_R^2 = \frac{N}{2} , \quad \sigma_{R_u}^2 = 2\pi^2 N\langle x_n^2\rangle , \quad \sigma_{R_v}^2 = 2\pi^2 N\langle y_n^2\rangle , \tag{15}$$

and the average number of zeros per area becomes

$$M = \frac{1}{2\pi}\left(\frac{2}{N}\right)(2\pi^2 N)\sqrt{\langle x_n^2\rangle\langle y_n^2\rangle} = 2\pi\sqrt{\langle x_n^2\rangle\langle y_n^2\rangle} , \tag{16}$$

where $\langle x_n^2\rangle$ is the second moment of the $x$-coordinate of the impulse positions and $\langle y_n^2\rangle$ is the corresponding second moment of the $y$-coordinates.

If it is assumed that the impulses are uniformly distributed within a rectangular window of size $W_x \times W_y$, then the average number of zeros per area is

$$M = (\pi/6)W_xW_y . \tag{17}$$

It is noteworthy that this expression for the average number of zeros per area, $M$, is independent of $N$, the number of impulses in the blur function. Rather the average number of zeros is governed by the distribution of the impulses.

Fig. 7 contains a plot of the number of zeros of the transfer function versus the area of the window enclos-

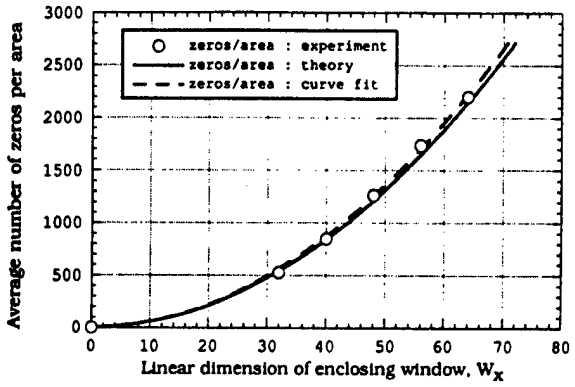


Fig. 7. Dependence of the average number of zeros per unit area for the random-walk transfer function on the size of the window enclosing the impulses. The solid curve is the theoretical result obtained from Eq. (16) and the dashed curve is the best-fit result for the experimental data points shown as the symbols. Note that the average number of zeros is independent of the number of impulses in the blur function.

ing the impulses. Included in the plot are the experimental results for six values of the area, the theoretical estimate from Eq. (17), and a minimum chi-squared fit [23] to the experimental data using the expression

$$\text{curve fit} = \frac{\pi}{\alpha} W_x W_y , \tag{18}$$

where the best-fit value of $\alpha$ was found to be 5.8 as opposed to the value of 6.0 of Eq. (17). It is seen in this plot that there is excellent agreement between the theoretical calculation and experimentally obtained results.

An important result of this research is realizing that there is a small likelihood of encountering a zero when sampling the transfer function for the image recovery process. Hence it is worthwhile to consider an approximate illustrative calculation of the probability per frame of encountering a zero in the transfer function. For the image recovery, consider sampling the transfer function on a lattice of $512 \times 512$ pixels and the frame to be of unit area. If due to noise fluctuations, we take the transfer function $B(f_x, f_y)$ to be zero in a tiny region around each discrete zero, i.e., an infinitesimal area $\Delta f_x \times \Delta f_y$ that is $(2 \times 10^{-6})^2$, then the probability, $P$, of encountering a zero is approximately

$$P = M(512)^2(2 \times 10^{-6})^2 , \tag{19}$$

where $M$ is the average number of zeros. In the blurred bird of Fig. 2, the blur function impulses were enclosed in a window of size $64 \times 64$ pixels. From the curve shown in Fig. 7, there will be approximately 2200 zeros in the transform space and therefore the probability, of encountering a zero is given by

$$P = 2200(512)^2(2 \times 10^{-6})^2 = 1/433 . \tag{20}$$

Thus, for this case, a zero will be encountered in the transform domain once in every 433 frames. In a typical set of computer simulations (50 different MPIR), we recover images of the high quality shown in Fig. 3.

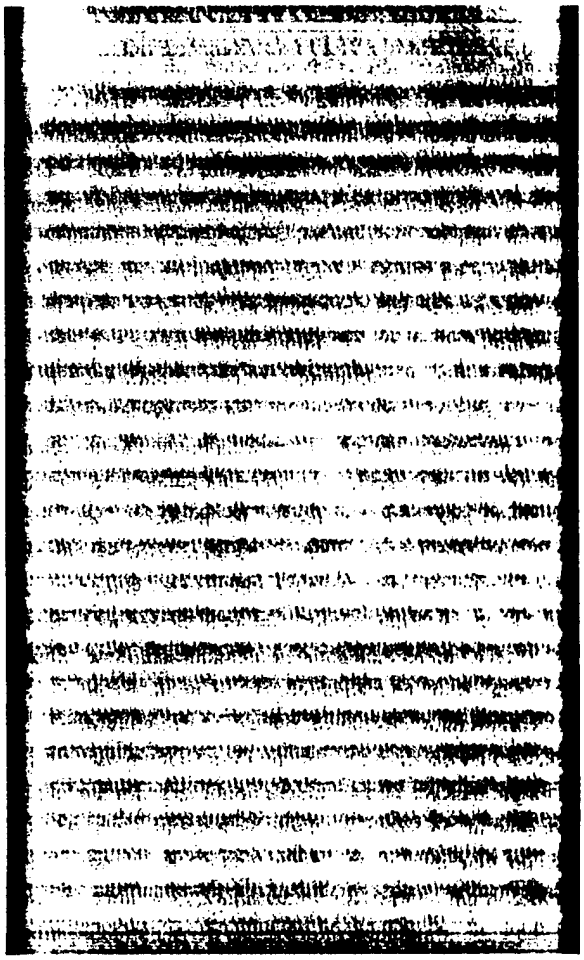

Fig. 8. Text image blurred with a 50-point impulse response. The original image contains $512 \times 1024$ pixels and the text is no longer readable.

## 5. Coding of textual images

To investigate the effects of blurring textual images, an independent MPIR was used to construct the blurred/coded image of Fig. 8. In this experiment a page of text is digitized and blurred using a 50-point MPIR. The positions of the impulses are restricted to lie within a $64 \times 64$ pixel window centered on the origin and are chosen from a computer generated ensemble of uniformly distributed random numbers. One can see that the MPIR has coded the text beyond recognition. The reconstructed image, using the appropriate generalized inverse filter, is shown in Fig. 9. There is only negligible error between the original scanned image and the recovered image.

From Figs. 2 and 8, the controlled blur is seen to be a technique for obtaining privacy or coding in image transmission. We have investigated the degree to which privacy is achieved by reconstructing the blurred bird using 20 points correctly positioned and 5 points chosen at random. Under these conditions the image recovery gives barely perceptible results. For 17 points correctly located and 8 in error, the recovered bird is not recognizable.

We have obtained excellent reconstructions of images that have been degraded by the multiple-point impulse response, which consists of irregularly positioned impulses. The blurred bird and the recovery are shown in Figs. 2 and 3, respectively. It is found that, although the zeros of the real and imaginary parts of the transfer function form closed, continuous contours, zeros of the transfer function occur at discrete locations and do not have a deleterious effect on the reconstructions.

**LINCOLN'S GETTYSBURG ADDRESS**

"Fourscore and seven years ago our fathers brought forth on this continent a new nation, conceived in liberty, and dedicated to the proposition that all men are created equal. Now we are engaged in a great civil war, testing whether that nation, or any nation so conceived and so dedicated, can long endure. We are met on a great battlefield of that war. We have come to dedicate a portion of that field, as a final resting place for those who here gave their lives that that nation might live. It is altogether fitting and proper that we should do this. But, in a larger sense, we cannot dedicate—we cannot consecrate—we cannot hallow—this ground. The brave men, living and dead, who struggled here, have consecrated it, far above our poor power to add or detract. The world will little note, nor long remember, what we say here, but it can never forget what they did here. It is for us the living, rather, to be dedicated here to the unfinished work which they who fought here have thus far so nobly advanced. It is rather for us to be here dedicated to the great task remaining before us,—that from these honored dead we take increased devotion to that cause for which they gave the last full measure of devotion—that we here highly resolve that these dead shall not have died in vain—that this nation, under God, shall have a new birth of freedom—and that government of the people, by the people, for the people, shall not perish from the earth."

Fig. 9. Text image reconstructed using an appropriate generalized inverse filter for the 50-point impulse response used to generated Fig. 8. The original scene has been faithfully recovered and the text is again readable.

## References

[1] J.L. Harris, J. Opt. Soc. Am. 56 (1966) 569.
[2] C.W. Helstrom, J. Opt. Soc. Am. 57 (1967) 297.
[3] T.S. Huang, ed., Picture Processing and Digital Filtering (Springer, Berlin, 1983) pp. 177–248.
[4] B.J. Stossel, Image processing, coding, and compression with multiple-point impulse response functions, Ph.D. thesis, Univ. Rochester, Rochester, NY (1994).
[5] N. George and B.J. Stossel, patent application granted, Serial No. 08/154311 (Filed 1993).
[6] M.I. Sezan and A.M. Tekalp, IEEE Trans. Acoust., Speech, Signal Proc. 38 (1990) 181.
[7] G. Arfken, Mathematical methods for physicists, 3rd Ed. (Academic Press, San Diego, 1985).
[8] M.Z. Nashed, Aspects of generalized inverse in analysis and regularization, in: Generalized inverses and applications, ed. M.Z. Nashed (Academic Press, San Diego, 1976).
[9] A.N. Tikhonov and V.Y. Arsenin, Solutions of ill-posed problems (J. Wiley, New York, 1977).
[10] H. Lipson and C.A. Taylor, Fourier transforms and x-ray diffraction (G. Bell and Sons, London, 1958).
[11] B.J. Thompson, Optical transforms and coherent processing systems with insights from crystallography, in: Optical Data Processing, ed. D. Casasent (Springer-Verlag, Berlin, 1978).
[12] J.F. Nye and M.V. Berry, Proc. Royal Soc. London A 336 (1974) 165.
[13] N.B. Baranova and B.Ya. Zel'dovich, Sov. Phys. JETP 53 (1981) 925.

[14] N.B. Baranova, B.Ya. Zel'dovich, A.V. Mamaev, N.F. Philipetskii and V.V. Shkunov, Sov. Phys. JETP 56 (1982) 983.
[15] S.O. Rice, Selected papers on noise and stochastic processes, ed. N. Wax (Dover, New York, 1954).
[16] J.W. Strutt (Lord Rayleigh), On the resultant of a large number of vibrations of the same pitch and of arbitrary phase, Phil. Mag. 10 (1880) 73.
[17] D. Middleton, Introduction to statistical communication theory (McGraw-Hill, New York, 1960).
[18] B.V. Gnedenko and A.N. Kolmogorov, Limit distributions for sums of independent random variables (Addison-Wesley, Massachusetts, 1968).
[19] P.N. Pusey, Statistical properties of scattered radiation, in: Photon correlation Spectroscopy and velocimetry, eds. H.Z. Cummins and E.R. Pike (Plenum Press, New York, 1977).
[20] J.W. Strutt (Lord Rayleigh), On the problem of random vibrations, and of random flights in one, two, or three dimensions, Phil. Mag. 37 (1919) 321.
[21] P.N. Pusey, D.W. Schaefer and D.E. Koppel, J. Phys. A 7 (1974) 530.
[22] B.R. Frieden, Probability, statistical optics, and data testing (Springer, Berlin, 1983).
[23] P.R. Bevington, Data reduction and error analysis for the physical sciences (McGraw-Hill, New York, 1969).

ELSEVIER

1 January 1997

Optics Communications 133 (1997) 22–26

OPTICS COMMUNICATIONS

# Lensless electronic imaging

Nicholas George [1]

*The Institute of Optics, University of Rochester, Rochester, NY 14627, USA*

Received 6 June 1996; accepted 4 July 1996

**Abstract**

A theory is presented for image retrieval when a planar transparency is illuminated by spatially incoherent light that propagates in free space and is then recorded on a CCD array, but without using an imaging lens. Based on Maxwell's equations and Fourier-optical, linear-systems theory, equations are derived for digital processing of this badly blurred image in order to recover a reasonable facsimile of the original. Rigorous impulse responses and their corresponding transfer functions are presented for the cases of general amplitude illumination and for incoherent illumination.

## 1. Introduction

Image processing methods have been applied to remove blur due to motion, degradation due to diffraction limits, and blur due to poor focus [1,2]. As computing power has increased, these methods are being more widely applied to include correction for known aberrations and image recovery using partial information [3]. A recent study showed that blur caused by an impulse response consisting of irregularly spaced impulses could be completely removed [4,5]. Since the corresponding transfer function contains only discrete, countable zeros, it is found that either a simple inverse filter or a Weiner-Helstrom filter [6] yields good results.

In this paper we consider the feasibility of image recovery when the image blur is due to diffraction spreading through open space without the use of a lens, as in Fig. 1. Restating, we consider whether it is possible to retrieve an image at a remote location from an incoherently illuminated object transparency that is located in the plane at $z = 0$. No lens is used for forming an image, and the badly blurred recording is made electronically by a CCD array at a distance $z = d$. For the theory, an analytic signal notation is used so that signals of arbitrary bandwidth can be included, and traveling waves appear in an exponential form. We consider a plane-polarized scalar component of the real-valued electric

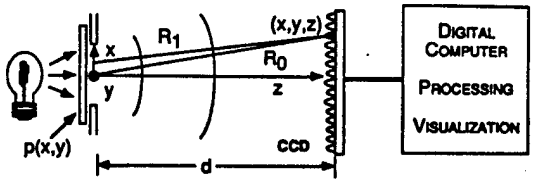


Fig. 1. Basic setup for the theory showing an input transparency $p(x, y)$ in the plane $z = 0$. The output intensity is recorded at $z = d$ after lensless, free-space propagation.

[1] E-mail: ngeorge@troi.cc.rochester.edu.


*PII* S0030-4018(96)00469-5

field, denoted by $\mathscr{E}_y^{(r)}(x, y, z; t)$. Time truncation rect$(t/T)$ is used so the temporal Fourier transform, $E_y(x, y, z; \nu)$, is defined by

$$E_y(x, y, z; \nu) = \int_{-\infty}^{\infty} \mathscr{E}_y^{(r)}(x, y, z; t) \times \mathrm{rect}(t/T)\, \exp(-\mathrm{i}2\pi\nu t)\, \mathrm{d}t, \tag{1}$$

where $(x, y, z)$ are Cartesian coordinates for an arbitrary point, $\nu$ is the temporal transform variable, and the lim $T \to \infty$ notation is implicitly understood. The signal representations used in this paper follow closely that in the literature and are reviewed more fully in Refs. [7,8] in the context of diffraction integrals based on Maxwell's equations. From Eq. (1), the corresponding analytic signal, denoted by the subscript 'a' in $E_{ya}(x, y, z; \nu)$, is defined as containing only the positive frequency components as follows:

$$E_{ya}(x, y, z; \nu) = E_y(x, y, z; \nu)[1 + \mathrm{sgn}(\nu)]. \tag{2}$$

The symmetrical step-function, sgn$(\nu)$ is defined by

$$\mathrm{sgn}(\nu) = 1, \quad \text{when } \nu > 0, \qquad = -1, \quad \text{when } \nu < 0. \tag{3}$$

From the Fourier inversion formula and Eq. (2), we can write the time-dependent analytic form $\mathscr{E}_{ya}(x, y, z, t)$ corresponding to $\mathscr{E}_y^{(r)}$ as

$$\mathscr{E}_{ya}(x, y, z, t) = \int_{-\infty}^{\infty} E_{ya}(x, y, z; \nu) \times \exp(+\mathrm{i}2\pi\nu t)\, \mathrm{d}\nu.$$

One can also readily verify a well-known alternative equation that is handy for computing $\mathscr{E}_y^{(r)}(x, y, z, t)$ from the analytic form, viz.,

$$\mathscr{E}_y^{(r)}(x, y, z, t) = \left[\mathscr{E}_{ya}(x, y, z, t) + \mathscr{E}_{ya}^{*}(x, y, z, t)\right]/2. \tag{4}$$

## 2. Linear system theory and diffraction integrals

Now for the problem at hand, as shown in Fig. 1, we will shortly see that it is possible to provide an exact solution of Maxwell's equations using the idealizations inherent in the model. Using the Rayleigh-Sommerfeld-Smythe form for the radiation in the right-half-space expressed in terms of the "known" tangential electric field in the plane at $z = 0$, we can write the exact solution, as follows [8,9]:

$$E_{ya}(x, y, z; \nu) = \frac{1}{2\pi} \iint_{-\infty}^{\infty} \mathrm{d}x'\, \mathrm{d}y'\, E_{ya}(x', y', 0; \nu) \times \frac{\exp(-\mathrm{i}kR_1)}{R_1} \left(\frac{z}{R_1}\right)\left(\mathrm{i}k + \frac{1}{R_1}\right), \tag{5}$$

in which

$$R_1 = \left[(x - x')^2 + (y - y')^2 + z^2\right]^{1/2}, \tag{6}$$

and $k = 2\pi\nu/c$ where $c = 3 \times 10^8$ m/s. One can write a similar equation for $E_{xa}(x, y, z; \nu)$ in terms of $E_{xa}(x', y', 0; \nu)$ and then a separate form for $E_{za}(x, y, z; \nu)$ in terms of the tangential aperture fields $E_{xa}(x', y', 0; \nu)$ and $E_{ya}(x', y', 0; \nu)$. These three equations for $E_{xa}$, $E_{ya}$, and $E_{za}$ comprise an exact solution in integral form for Maxwell's equations for radiation from a planar aperture. Eq. (5) forms the basis for the calculation of radiation from an aperture. Typically one considers a blocking function and the source illumination which are implicit in the scalar component of the electric field in the aperture, $E_{ya}(x', y', 0; \nu)$.

The linear system interpretation of Eqs. (5) and (6) is to notice that the output scalar amplitude is given by a convolution of the input scalar amplitude with the impulse response $h(x - x', y - y'; \nu)$. Hence, we can write that

$$h(x - x', y - y'; \nu) = \frac{\exp(-\mathrm{i}kR_1)}{2\pi R_1} \left(\frac{z}{R_1}\right)\left(\mathrm{i}k + \frac{1}{R_1}\right), \tag{7}$$

in which $R_1$ is given by Eq. (6). Since this impulse response is space-invariant, we write the following simpler form:

$$h(x, y; \nu) = \frac{\exp(-\mathrm{i}kR_0)}{2\pi R_0} \left(\frac{z}{R_0}\right)\left(\mathrm{i}k + \frac{1}{R_0}\right), \tag{8}$$

in which the distance to $x, y, z$ from the origin, $R_0$, is given by

$$R_0 = \left(x^2 + y^2 + z^2\right)^{1/2}. \tag{9}$$

Consider an input transparency $p(x, y)$ placed in the plane at $z=0$ and illuminated by a plane-polarized beam $E_{ya0}(x', y', 0^-; \nu)$ incident from the left in Fig. 1. Making the usual Kirchhoff approximation, we set $E_{ya}(x', y', 0; \nu)$ as follows:

$$E_{ya}(x', y', 0; \nu) = p(x, y)\, E_{ya0}(x', y', 0^-; \nu). \tag{10}$$

For incoherent illumination, we briefly summarize the calculation. Denoting the blurred output scene recorded at $z=d$ by $u_2(x, y; \nu)$, we calculate the expected value of the density of energy in the electric field over an ensemble of sources, viz.,

$$u_2(x, y; \nu) = \lim_{T\to\infty} \left\langle \frac{E_{ya}(x, y, d; \nu) E_{ya}^*(x, y, d; \nu)}{T} \right\rangle. \tag{11}$$

The source description for incoherent illumination is given by a delta-function form as follows:

$$\lim_{T\to\infty} \left\langle \frac{E_{ya0}(x', y', 0^-; \nu) E_{ya0}(x'', y'', 0^-; \nu)}{T} \right\rangle = \delta(x'-x'')\,\delta(y'-y'')\,S_1(\nu), \tag{12}$$

in which the input illumination spectral density $S_1(\nu)$ is defined by an ensemble average over the sources as

$$S_1(\nu) = \lim_{T\to\infty} \left\langle \frac{|E_{y0}(x', y', 0^-; \nu)|^2\, A_0}{T} \right\rangle, \tag{13}$$

in which $A_0$ is an infinitesimal area of coherence. The blurred image recorded at the CCD is given by calculation of Eq. (11) substituting Eqs. (5) and (12) and integrating over the input plane. In a linear system formalism, we write the blurred image recorded at the CCD array ($z=d$) as a convolution of the input picture intensity transmittance with the impulse response for incoherent illumination. The result is given by

$$u_2(x, y; \nu) = p(x, y)\, p^*(x, y) * h(x, y; d) \times h^*(x, y; d) S_0(\nu), \tag{14}$$

where the asterisk $*$ denotes a two-dimensional convolution over $(x, y)$.

Interestingly, by Eqs. (8) and (9) into (14), we find the exact expression for the impulse response due to free space propagation from an incoherently illuminated planar aperture, as follows:

$$|h(x, y; d; \nu)|^2 = \left(\frac{1}{2\pi}\right)^2 \frac{d^2}{(x^2+y^2+d^2)^2} \left(k^2 + \frac{1}{x^2+y^2+d^2}\right). \tag{15}$$

The $\exp(-ikR_1)$ terms in Eq. (5) have cancelled due to the delta correlation of the source. Hence, in Eqs. (14) and (15) the solution is not limited to the usual paraxial and $z$-distance limitations inherent in the Fresnel-zone case [10]. Moreover, we recognize in Eq. (15) that the first member on the right ($k^2$) is the dominant term in the propagation once we are a few wavelengths from the aperture. The second term $[1/(x^2+y^2+d^2)]$ is the near zone term and it is important in the limiting case as $z$ goes to zero, say, in Eq. (5).

## 3. Image recovery for free-space propagation

In Fourier optics with incoherent illumination, one characterizes a space-invariant linear optical system by an impulse response and a corresponding optical transfer function. The Fourier transform of the blurred picture at $z=d$ is denoted by $U_2(f_x, f_y; \nu)$ and defined by

$$U_2(f_x, f_y; \nu) = \iint_{-\infty}^{\infty} dx\, dy\, u_2(x, y; \nu) \times \exp[-i2\pi(f_x x + f_y y)], \tag{16}$$

where $(f_x, f_y)$ are spatial transform variables for $(x, y)$. The spatial frequency response formula for free space propagation is obtained by taking the two-dimensional transform of Eq. (14). The result is given by a simple product of the Fourier transform of object intensity and the optical transfer function, as follows:

$$U_2(f_x, f_y; \nu) = \mathcal{F}|p(x, y)|^2 \cdot \mathcal{F}|h(x, y; d, \nu)|^2 \cdot S_0(\nu), \tag{17}$$

Table 1
Impulse response and transfer functions for free-space propagation from a planar aperture at $z = 0$ into the right-half-space. For the general amplitude transfer function, select the positive square root when $f_x^2 + f_y^2 < (k/2\pi)^2$ and the negative imaginary value when $f_x^2 + f_y^2 > (k/2\pi)^2$ to include only damped evanescent waves in the latter case

| System description input | Impulse response | Transfer function |
|---|---|---|
| General case amplitude input $p(x, y; \nu)E_{y\alpha 0}(\nu)$ | $[\exp(-ikR_0)/2\pi R_0](z/R_0)(ik + 1/R_0)$ | $\exp\{-i2\pi z[(k/2\pi)^2 - f_x^2 - f_y^2]^{1/2}\}$ |
| Incoherent illumination intensity case $\lvert p(x, y; \nu)\rvert^2 S_0(\nu)$ | $[z^2/(2\pi)^2 R_0^4](k^2 + 1/R_0^2)$ | $(k^2 z f_\rho K_1/2)(2\pi df_\rho) + (\pi f_\rho^2 K_2/4)(2\pi df_\rho)$ |

Notation: $R_0^2 = x^2 + y^2 + z^2$ and $f_\rho^2 = f_x^2 + f_y^2$

in which the operator $\mathcal{F}$ denotes the two dimensional spatial transform over $(x, y)$. To calculate the Fourier transform of $|h(x, y; d; \nu)|^2$ we notice the cylindrical symmetry in Eq. (15) and obtain the result with two applications of Eq. (6.565.4) of Ref. [11]. The resulting optical-transfer-function for free space propagation from $z = 0$ to $d$ is given by

$$\mathcal{F}|h(x, y; d; \nu)|^2 = \frac{k^2 df_\rho}{2} K_1(2\pi df_\rho) + \frac{\pi f_\rho^2}{4} K_2(2\pi df_\rho), \quad (18)$$

in which the cylindrical spatial frequency, $f_\rho$, is defined by

$$f_\rho = \left(f_x^2 + f_y^2\right)^{1/2}. \quad (19)$$

$K_1(2\pi df_\rho)$ and $K_2(2\pi df_\rho)$ are the modified Bessel functions of the second kind of order one and two, respectively.

One clearly sees the dominance of the first member in Eq. (18) by the ratio of their coefficients which is $8\pi d/(\lambda^2 f_\rho)$. With $\lambda = 0.5$ $\mu$m, $d = 10$ mm, $f_\rho = 10$ $c$/mm this ratio is roughly $10^8$. It is instructive to plot $K_1(2\pi df_\rho)$ on a logarithmic scale as in Fig. 2. From this, we see that $K_1(2\pi df_\rho)$ is infinite at the origin and drops exponentially to zero for infinite argument. This is clear from the following expressions valid for small arguments, from Eq. (9.6.9) in Ref. [12]:

$$K_1(v) \cong 1/v \quad \text{and} \quad K_2(v) \cong 2/v^2, \quad (20)$$

as $v$ goes to zero. By Eq. (20) it is clear that the transfer function in Eq. (18) is finite as $(df_\rho) \to 0$. And at large values for their arguments, the modified Bessel functions of the second kind have the following expression:

$$K_n(v) \cong (\pi/v)^{1/2} e^{-v}. \quad (21)$$

Most interestingly, the modified Bessel functions $K_n(v)$ do not have any finite zeros for real arguments. With reference to Eq. (17), this makes the blurred image $U_2(f_x, f_y; \nu)$ a prime candidate for image retrieval, i.e., recovering $\mathcal{F}|p(x, y)|^2$ and hence the image intensity $|p(x, y)|^2$, since the Fourier transform of the blurring function, $\mathcal{F}|h|^2$, has no zeros in the real frequency plane $(f_x, f_y)$. Due to the absence of zeros in the transfer function but with the inclusion of noise, it is hopeful that the Weimer-Helstrom modified inverse filter would be an appropriate start. As pointed out in our earlier

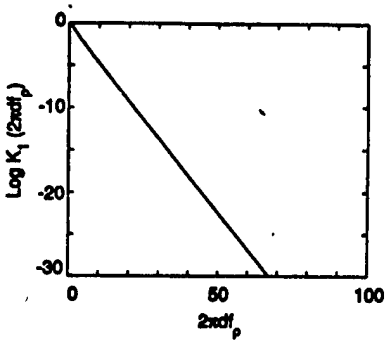


Fig. 2. The modified Bessel function $K_1(2\pi df_\rho)$ plotted logarithmically versus the argument. The plot starts at $2\pi df_\rho = 1$ in order to avoid the singularity at the origin.

article [5], this type of inversion problem to recover $|p(x, y; \nu)|^2$ is ill-posed, and it may well need some means of regularization which is beyond the scope of this article [13,14].

## 4. Summary

In this paper we have presented the exact impulse responses for free-space propagation into the right-half-space from an idealized planar aperture, see Table 1 and Eqs. (7) and (15) for the cases of amplitude illumination and incoherent illumination, respectively. With exact results in the framework of Maxwell's equations, we find that free-space propagation from a planar aperture is space-invariant in general. One main theme is to derive a rigorous expression for the optical-transfer-function of free space, and thereby secondly to study the feasibility of image retrieval using a lensless recording system and post digital processing. We find the interesting result that this intensity based transfer function in Eq. (18) consists principally of a modified Bessel function of the second kind, $K_1(v)$, which is well-known not to have any zeros for finite real values of its argument. The significance of this is that recovery of the pictorial image, $|p(x, y; \nu)|^2$, is likely using digital processing means.

## References

[1] T.S. Huang, ed., Picture Processing and Digital Filtering (Springer, Berlin, Second Edition, 1979) pp. 177–288.
[2] A.K. Jain, Fundamentals of Digital Image Processing (Prentice Hall, Englewood Cliffs, 1989).
[3] H. Stark, Image Recovery: Theory and Application (Academic Press, Orlando, 1987).
[4] N. George and B.J. Stossel, U.S. Patent No. 5,453,844.
[5] B.J. Stossel and N. George, Optics Comm. 121 (1995) 156.
[6] C.W. Helstrom, J. Opt. Soc. Am. 57 (1967) 297.
[7] L.G. Shirley and N. George, J. Opt. Soc. Am. A 4 (1987) 734.
[8] R.E. English and N. George, Appl. Opt. 26 (1987) 2360.
[9] W.R. Smythe, Static and Dynamic Electricity (Summa-Hemisphere, New York, Third Edition, revised, 1989) p. 448–482.
[10] J.W. Goodman, Introduction to Fourier Optics (McGraw-Hill, New York, 1968).
[11] I.S. Gradshteya and I.M. Ryzhik, Table of Integrals, Series, and Products (Academic Press, New York, 1965) pp. 686, 952, 958.
[12] M. Abramowitz and I.A. Stegun, Handbook of Mathematical Functions (Nat. Bur. of Stds., Washington D.C., 1964) pp. 374–379.
[13] M.Z. Nashed, Aspects of generalized inverse in analysis and regularization, in: Generalized inverses and applications, ed. M.Z. Nashed (Academic Press, San Diego, 1976).
[14] A.N. Tikhonov and V.Y. Arsenin, Solutions of ill-posed problems (Wiley, New York, 1977).